Canadian Science Publishing | Canadian Journal of Civil Engineering

RHS Webs under Transverse Compression

Journal:	*Canadian Journal of Civil Engineering*
Manuscript ID	cjce-2018-0485.R1
Manuscript Type:	Article
Date Submitted by the Author:	28-Nov-2018
Complete List of Authors:	Kuhn, Jens; Schlaich Bergermann Partner Packer, Jeffrey; University of Toronto, Civil Engineering Fan, YuJing; COWI North America Ltd
Keyword:	structure - steel < Struct.Eng. & Constr.Mate, MP - steel < Engineering Materials
Is the invited manuscript for consideration in a Special Issue? :	Not applicable (regular submission)

RHS WEBS UNDER TRANSVERSE COMPRESSION

by

Jens Kuhn[1], Jeffrey A. Packer[2*] and YuJing Fan[3]

[1]Schlaich Bergermann Partner, Schwabstrasse 43, 70197 Stuttgart, Germany

[2]Department of Civil & Mineral Engineering, University of Toronto, 35 St. George Street, Toronto, ON, M5S 1A4, Canada

[3]COWI North America Ltd., 101-788 Harbourside Drive, North Vancouver, BC, V7P 3R7, Canada

Abstract

An investigation is presented into full-width, RHS X-connections subject to transverse compression, including the effect of a compressive or tensile chord preload. A re-evaluation of world-wide experimental tests on full-width X-connections revealed considerable inaccuracy with current design recommendations, as well as significant discrepancies between them. A finite element study was hence conducted to further investigate the behaviour of such connections. A critical value of the bearing length-to-chord height ratio was found, where yielding failure of the chord webs turns into buckling failure, and this has been implemented in the subsequent design recommendation. The proposed design procedure is based on 350 finite element results, covering a wide range of chord sidewall slenderness values, bearing length values and chord stress ratios, as well as against a screened data base of 125 experimental tests. The proposal is shown to offer excellent predictions and incorporates a simple reliability analysis.

Keywords

Steel structures, hollow structural sections, rectangular hollow sections, truss connections, welded joints, web buckling, web crippling, static strength, numerical modelling

* Corresponding author, email: jeffrey.packer@utoronto.ca

Introduction

A large number of research projects have now been performed worldwide to investigate the behaviour of welded rectangular hollow section (RHS) connections under predominantly static loads. The results have led to a number of contemporary internationally recognized design recommendations, such as ISO 14346 (ISO 2013), CIDECT Design Guide No. 3, 2nd edition (Packer et al. 2009) and Wardenier et al. (2010). In addition, RHS connection design rules are prescribed by prominent normative codes such as EN 1993-1-8 (CEN 2005) and AISC 360-16 (2016), as well as the informative CISC Design Guide, 2nd edition (Packer and Henderson 1997).

Experimental test data from research work all over the world on full-width RHS-to-RHS X-connections (sometimes referred to as cross-connections), loaded in branch compression, has been collected in the past and compared to design standards at that time (Packer 1984; Packer 1987). These studies revealed that predictive equations in codes for web compression failure were quite inaccurate. Some analytical research into such connections (Davies and Packer 1987) has shown that the bearing length (relative to the chord height) has an interaction with the slenderness of the chord wall under compression, and that these two parameters jointly determine whether the connection fails by sidewall yielding or buckling. Recently, the experimental database of compression-loaded, full-width, RHS-to-RHS and plate-to-RHS X-connections has been re-visited and expanded (Fan 2017), and again evaluated against contemporary design standards. This has revealed that current standards in North America (AISC 2016; CSA 2014) are often unsafe, yet Eurocode 3 (CEN 2005) and CIDECT design recommendations (Packer et al. 2009) give safe but very uneconomical (excessively conservative) predictions.

Thus, a resolution of the dilemma surrounding the web capacity of transversely compressed RHS is highly desirable. Since experimental investigations are expensive and time-consuming, companion numerical "tests" are often carried out to generate a large additional database, which is the approach adopted herein. Currently, the effect of the chord normal stress on the ultimate capacity of RHS connections is also a point of contention. Therefore, the numerical modelling presented also covers the influence of compressive and tensile chord stresses on transversely compressed RHS webs. In addition to RHS-to-RHS X-connections, transverse plate-to-RHS connections are investigated; hence the important effect of "bearing length" on sidewall capacity is studied. Based on the experimental and numerical evidence, a proposal is presented which allows a safe yet efficient

design of full-width RHS X-connections under branch compression, with branches being welded or unwelded to the chord.

State of the Art of RHS X-Connection Design

The scope of this review covers the design recommendations used in Europe, the USA and Canada, and recommendations available in international consensus guides. Important knowledge pertaining to the behaviour of RHS X-connections, which are characterized by a force being transferred from one side of the RHS chord to the other, is also noted. The connection limit states are described in different ways for the variety of design codes which are summarized here. Figs. 1 and 2 show the notation used for axially loaded RHS-to-RHS X-connections with two opposing branches welded to the chord, as well as axially loaded transverse plate-to-RHS X-connections.

Basis for design of RHS webs in compression

RHS connections achieve their highest strength with a branch-to-chord width ratio (β) of 1.0 due to the higher stiffness of the webs compared to a much softer connection when β is smaller than unity. The concentrated load can then be directly transmitted to the RHS webs without bending of the flanges. When concentrated loads are transferred directly to the RHS webs by equal-width RHS branch members, or I-beam flanges or plates, the connection capacity is limited by sidewall failure. Unlike most current design codes, CSA S16-14 (2014) includes web crippling (a local buckling failure directly beneath the flange) as a possible failure mode for RHS X-connections, and AISC 360-16 (2016) includes web crippling for RHS T- and Y-connections. The latter (outside the scope of this paper) are defined by the branch axial load being equilibrated by beam shear in the chord member. However, as noted in the Commentary to AISC 360-16 Section J10.3 (AISC 2016), web local crippling provisions were derived from tests on I-section beams; the only application checked for hollow sections involved box sections with slender webs.

In Table 1, design provisions from the North American structural steel design standards/specifications, CIDECT Design Guide No. 3 2nd edition (which is identical to ISO 14346) and Eurocode 3 (EN 1993-1-8), are summarized and compared to each other. In all cases the connection is presumed to be remote from an open

chord end, so that it is not influenced by "chord end effects". A significant variation between the design rules is evident.

Of note in Table 1 is the depiction of full-width X-connection behaviour in North American codes, where multiple limit states need to be checked for web compression failure. The minimum resistance predicted by web yielding, web buckling and web crippling failure governs for CSA S16-14. The web crippling failure mode stands out though, because RHS member sizes usually do not reach the high sidewall slenderness ratio (h_0/t_0) where web crippling failure may govern. Crippling failure is better known in deep I-shaped sections, where the web deforms out of plane locally under the flange when loaded by a concentrated force. As far as is known from past experiments, true web crippling failure has never occurred for a full-width RHS X-connection under transverse compression, although this term has been used loosely in the past to describe many forms of RHS web compression failure. Moreover, in North American codes plate buckling equations are used to describe RHS web buckling behaviour, whereas most other international design recommendations tend to use an equivalent column buckling equation. The Commentary to AISC 360-16 Section J10.5 (AISC 2016) at least notes that this North American approach to web buckling is inappropriate if the bearing length-to-RHS depth ratio "is not small" and this ratio is approximately ≥ 1.

CIDECT DG3 (Packer et al. 2009), ISO 14346 (ISO 2013) and EN 1993-1-8 (CEN 2005) assume a 1:2.5 load dispersion through the chord thickness to create a loaded effective width. Web failure by yielding or buckling is then determined by a buckling coefficient. For stocky chord specimens yielding failure governs, for slender chord cross sections buckling. Implicit in the Eurocode 3, CIDECT and ISO method is a standardized "column effective width", regardless of the connection failure mode (yielding versus buckling). For yielding failure of the connection, the different codes are in agreement, with the exception of CSA S16 (2014) where a different load dispersion slope is assumed.

A significant difference between the codes lies in the way the influence of chord force on the connection strength is taken into account, by the reduction factor Q_f or k_n (see eqs. (1) and (2)). CIDECT/ISO reduce the connection strength for chord tension and compression stress, whereas all other design standards and recommendations only reduce connection strength under chord compression stress. Furthermore, in the case of

yielding failure, AISC and CSA provide no chord stress reduction factor, whereas Eurocode 3 and CIDECT/ISO do.

Influence of chord stress on connection capacity

In the current versions of the above-mentioned design recommendations, there are principally two reduction functions used to account for the effect of chord stress on RHS-to-RHS X-connections. These are the factor k_n (eq. (1)) according to EN 1993-1-8, and the factor Q_f (eq. (2)) according to CIDECT DG3.

(1) $$k_n = \begin{cases} 1.3 + \frac{0.4n}{\beta} \leq 1.0 & \text{Compression (n } < 0) \\ 1.0 & \text{Tension (n } > 0) \end{cases}$$

(2) $$Q_f = (1 - |n|)^{C_1} \text{ with } C_1 = \begin{cases} 0.6 - 0.5\beta & \text{Compression (n } < 0) \\ 0.1 & \text{Tension (n } > 0) \end{cases}$$

where n is the ratio of the chord stress at the connecting face to the chord yield stress.

C_1 is a constant of 0.1 for both compressive and tensile stresses in the chord, with full-width X-connections ($\beta = 1.0$), which results in a uniform reduction factor under both chord tensile and compressive loading. The biggest difference lies in the handling of chord tensile stress. CIDECT stipulates a reduction, based on Wardenier et al. (2007), whereas EN 1993-1-8 does not suggest any strength reduction for tensile loading of the chord. Further research has confirmed that a reduction is indeed necessary for chord tensile loading (e.g. Voth and Packer 2012; Lipp and Ummenhofer 2014; Wardenier et al. 2018). However, to date, no experimental data for chord tensile preloading is available for full-width RHS T- and X-connections. Therefore, CIDECT DG3 refers to the general function $Q_f = (1 - |n|)^{0.1}$ for RHS connections as a conservative lower bound, based on test results for RHS K-connections (see Wardenier et al., 2007).

For plate-to-RHS connections, CIDECT DG3 suggests a different reduction factor which is based on the numerical investigation of Lu (1997), valid for I-section beams and for transverse plates welded to RHS chords. This is given by eq. (3) and is illustrated in Fig. 3. Also shown in Fig. 3 is the RHS-to-RHS k_n factor from EN 1993-1-8 given by eq. (1).

(3) $$Q_f = (1 - |n|)^{C_1} \text{ with } C_1 = \begin{cases} 0.03\gamma & \text{Compression (n } < 0) \\ 0.1 & \text{Tension (n } > 0) \end{cases}$$

where n is the ratio of the chord stress at the connecting face to the chord yield stress.

Experimental Database

Prior experiments on full-width (β=1.0) X-connections under branch axial compression have been divided into three categories, as shown in Fig. 4: welded, unwelded, and welded on one side. This distinction is necessary because the connection capacity and the deformation profile of the chord differ for each situation. This effect of boundary conditions has been observed by Poloni (1985), and Zhao and Hancock (1992), who have tested RHS X-connections with different branch fixity. The branch welds (or lack thereof) create a different support condition for the chord sidewall. Welds between the branch and chord result in a much higher sidewall stiffness compared to specimens without welding. This allows one to assign different restraint conditions to the three different test setups. For example a modified web buckling equation could be used, where the chord sidewall end conditions with welds are classified as fixed supports, and as pinned supports if unwelded. If "welded on one side", the RHS corners cannot rotate where welded to a branch (a fixed support), but can rotate on the unwelded side where the specimen is reacted against a rigid base (a pinned support). There are thus three different restraint conditions for chord sidewalls under transverse compression in Fig. 4: (a) fixed-fixed; (b) pinned-pinned; and (c) fixed-pinned.

A database of 125 full-width, welded, welded on one side, and unwelded X-connections with branches/plates under axial compression, assembled from prior experiments undertaken in Canada, Europe and Australia, is given in Tables 8,9, and 10, plus the data for the two additional tests herein. The collected tests include chord sidewall slenderness (h_0/t_0) values ranging from 10 to 57, bearing lengths (h_1) from $0.04h_0$ up to $3.72h_0$, compressive stress in the chord up to 87% of the yield stress (f_y), branch-to-chord angles (θ_1) of 45°, 60°and 90°, as well as cold-formed, hot-finished and cold-formed stress-relieved RHS. "Equivalent branches", where steel blocks were welded to the chord, were also classified as welded connections, such as used in the tests by Poloni (1985). The influence of the size of the fillet weld between the chord flat and the branch was considered to be small, so weld size has been neglected. Source references for most tests in Tables 8, 9, 10 are given in Fan (2017), but Tables 8, 9, 10 also include additional experiments by Cheng and Becque (2016) and Serrano et al. (2017).

Additional Experiments for Validation of Finite Element Modelling

Two "welded on one side" RHS 90º X-connections were fabricated and tested to failure under displacement control, in quasi-static branch compression, as shown in Fig. 5, using a 5,000 kN-capacity universal testing machine. Although having the appearance of T-connections they would be classified for analysis as X-connections due to force transfer across the RHS chord member. As can be seen, the branch compression force is reacted by a steel pedestal, which was secured to the laboratory floor. This form of testing T-shaped specimens avoids supporting the chord member as a beam, which in turn induces chord face bending stresses into the connection region, whose influence is difficult to interpret (Packer et al. 2017). All members were made of cold-formed RHS. Two chord sizes (203x203x6.35 and 203x203x9.53) and one branch size (203x203x12.7) were used. The branch thickness was selected to be greater than that of the chord, to be certain that local branch yielding would not occur before the chord webs failed. The two test specimens have a β-ratio of 1.0 and two different chord wall slenderness ratios (2γ), nominally equal to 21 and 32. Measured geometric properties are given in Tables 2 and 3.

Mechanical properties of the chord members were determined by tensile tests on coupons cut from the RHS flat regions where there was no weld seam. Average measured values (using three coupons from each RHS) are shown in Table 4.

Both specimens failed by chord web buckling and the connection ultimate strength was given by the maximum load, $N_{1,u} = N_{1,max}$. Both specimens failed before the $3\%b_0$ connection ultimate deformation limit state (Lu et al. 1994) was reached, as can be seen on the connection load-displacement curves in Fig. 6. Displacements were determined by an optical camera system that recorded the global coordinates of light-emitting-diode (LED) targets positioned on the test specimens. To obtain the connection load-deformation curves in Fig. 6, the branch load was measured by the testing machine's load cell and vertical connection deformation was determined from the global vertical displacement of the LED located close to the connection (on the branch, 50 mm above the chord face).

Finite Element Modelling

In order to validate the finite element (FE) modelling procedure used herein, two RHS-to-RHS full-width X-connection FE models, reproducing the two experimental tests, were developed using ANSYS v18 (Swanson

Analysis Systems 2017). Planes of symmetry were used, whenever possible, to reduce the number of degrees of freedom. For modelling the two "welded on one side" test specimens, quarter models were used; for the subsequent parametric analysis of fully "welded" RHS-to-RHS X-connections, one-eighth models could be used, as shown in Fig. 7. The FE models assume that the X-connections are laterally supported against global out-of-plane displacement of the whole chord member.

Measured geometric properties of the test specimens were used for the FE models. With the branch under compression, the welds connecting the chord to the branch can be considered non-critical, but they were nevertheless modelled to closely replicate the physical shape. For this purpose, the measured fillet weld size in Table 2 was utilized for the welds transverse to the chord. The region between the corner radius of the chord and the branch was filled flush with a partial joint penetration flare-bevel groove weld (as in the experiments), which is important because this area is much stiffer than the chord flange and thus the majority of the load is transmitted through the chord webs.

Previous studies by Voth and Packer (2012) and van der Vegte et al. (2010) have confirmed the use of hexahedral elements as an appropriate way to capture hollow section connection behaviour under static loading. Hence, eight-noded brick elements (Solid185 in ANSYS element library), with three degrees of freedom per node and reduced integration and hourglass control, which are also suitable for nonlinear analysis, were utilized.

To model post-yield, large-deformation, non-linear behaviour the measured engineering stress-strain curves for the RHS material were converted to true stress-strain curves, using (Boresi and Schmidt 2003):

(4) $\sigma_T = \sigma(1 + \varepsilon)$

(5) $\varepsilon_T = ln(1 + \varepsilon)$

Engineering stress-strain curves, as well as the corresponding true stress-strain curve, are shown in Fig. 8 for the 203x203x9.53 RHS chord.

The FE boundary conditions for verification of the model were matched to the laboratory tests, in which there were two planes of symmetry due to the connection bearing on a rigid pedestal base on one side of the chord.

Displacements were imposed parallel to the branch incrementally by pressing the branch into the chord. A step-wise load application was selected to closely follow the nonlinear load-displacement curve and to ensure

convergence. The increments were set to 0.10 mm/step to ensure that the peak load was captured. To apply preload to the chord (in the subsequent parametric study), surface-based constraints were utilized. A surface-based constraint can be used to couple the motion of nodes on the contact surface (the chord end) to a single pilot node on the target surface. Forces applied on the pilot node are distributed to contact nodes through, in an average sense, shape functions. Therefore, a single node in the middle of the chord end surface was created and the preload was applied to that pilot node.

Sensitivity study and validation

The influence of the mesh size, the element type, the friction coefficient μ (for the pedestal support) and the number of elements through the RHS chord thickness were investigated. A sensitivity study was performed for both specimens.

Since the specimens were pushed against a pedestal in the experiments, to ensure a compression-only support for the FE model a contact area between the pedestal and the bottom of the specimen was created, which requires a friction coefficient. Typically, the friction coefficient between two steels varies between 0.3 (smooth) and 0.8 (rough), and the RHS-pedestal contact represents a rather smooth surface. Four different potential friction coefficients were examined to determine the most appropriate value. To ensure no other influences, for example mesh size or elements through the thickness, a fine mesh as well as four elements through the thickness were chosen for the friction coefficient study.

A sensitivity study was performed to determine the minimum mesh parameters necessary to obtain good results. Three different mesh densities were tested: fine, medium and coarse, which are illustrated in Fig. 9 for an RHS-to-RHS connection. By FE modelling standards for connections, the so-called “fine” mesh would generally be categorized as ultra-fine.

To determine the influence of elements through the thickness, two to five layers of elements through the thickness were examined in order to describe the chord sidewall buckling accurately. In addition, both 8-noded and 20-noded brick elements (Solid185 and Solid186 in ANSYS element library) were tested.

Tables 5 and 6 provide a summary of the analyses performed, showing the parameters that were varied as well as the ratio of the experimental ultimate load to the FE model ultimate load. As can be seen, the latter shows a relatively low scatter.

Within the bounds of the study, mesh density had very little influence on the results, so the coarse mesh density was adopted to reduce the number of elements. For the friction coefficient, a value of 0.3 was taken since this produced the best results compared to the other values in the range for the two specimens. Four elements through the thickness using 8-noded elements captured the buckling behaviour of the web well. Using this combination, a comparison of the load-displacement curves between the experiments and the FE model is shown in Fig. 10.

The overall load-deformation behaviour, the initial stiffness and the ultimate loads of the numerical and experimental results for the two specimens show good agreement. A small difference between the ultimate loads exists for the stocky specimen (Fig. 10(a)). Some differences can be attributed to residual stresses and different material characteristics in the corners of the test specimens. The ultimate load is of prime importance for this investigation and the load-deformation behaviour after the peak, or after 3% chord face indentation, is of less importance but it confirms the deformation capacity. The numerical models provide good predictions for the ultimate load $N_{1,u}$ and show good correspondence with the experimental curves up to the 3% displacement criterion.

In order to further confirm general agreement between the FE models and experiments, the deformations of the cross sections were compared. Tested connection specimens were cut through the middle of the branch and compared with the comparable FE-based model mirrored shape (see Fig. 11). Similar shapes are clearly visible. The unwelded flange on the bottom bends inward and the two chord sidewalls buckle outward. The picture of the experimental test shows much larger deformations because the specimens were tested up to a vertical connection deformation of about 20 mm. This is in an area where the material model for this FE analysis is no longer valid, hence the FE models were only “pressed” to a vertical connection deformation of 8 mm. Nevertheless, similarities can be clearly identified.

Numerical Parametric Study

A parametric study was carried out to generate additional numerical test data and to determine trends or influences of parameters on the connection capacity of full-width welded X-connections. All models used the same set of material properties, which were extracted from the average tensile coupon tests of the stocky specimen (X2). This provided real material behaviour for a cold-formed RHS which, as can be seen in Fig. 8, were converted to true stress-strain curves for use in ANSYS. The welds were modelled the same size as in the experiments, for all the parameter study, although the effect of the transverse fillet weld size on sidewall compression failure is negligible. To exclude branch failure in nearly all connections, due to the branch effective width phenomenon, a significantly thicker branch thickness (t_1 = 11 mm) was chosen. Connection failure was thus limited to chord web buckling and web local yielding. In addition, the angle θ_1 between the chord and the branch was constant (90°). Although the FE model was validated by two X-specimen (T-shaped) tests, pressed against a steel pedestal, X-connections with branches welded on both sides were used for the parametric study. This enabled the FE model to take advantage of another plane of symmetry, resulting in an one-eighth model. To remain in the range of validation with the two test specimens, and to sustain the mesh quality in the connection area – especially in the corner region where the chord corner and the branch corner intersect – the wall thickness of the chord t_0 was kept constant at 8 mm, which is between the two validation tests. As the investigation is aimed at determining the connection capacity of interior X-connections, the influence of end effects was eliminated by having sufficiently long chords. To generalize the corner radii of the RHS, $2t_i$ was used for the outer radius r_o, and t_i was used for the inner radius r_i. These are typical assumed values in North America, but they should have little influence on the connection capacity.

Based on the previously described connection properties, the parametric study determined the influences of chord sidewall slenderness (h_0/t_0 = 10, 20, 30, 40, 50), chord prestress (n = -0.75, -0.50, -0.25, 0, 0.25, 0.50, 0.75), and the branch height-to-chord width ratio (η = 2.0, 1.0, 0.5, 0.25, 0.10). This parameter combination also partially includes the influence of the branch height-to-chord height ratio, h_1/h_0, on the connection capacity. The branch-to-chord wall thickness ratio τ would only influence branch failure, due to the effective width phenomenon, but this failure mode was not intended to be produced in this numerical study. Hence, a numerical

investigation has not been carried out for the influence of the wall thickness ratio τ on the connection capacity, and for all RHS-to-RHS connections the branch-to-chord wall thickness ratio τ was set at 1.38.

Two connection arrangements were created with each having 175 models: one with a square chord and one with a rectangular chord. The rectangular chord set-up changes the chord height, h_0, and the branch height, h_1, with the remaining parameters staying constant. The square chord set-up changes the branch width, b_1, as well, when increasing the chord wall slenderness. The connection ultimate strengths, without chord prestress ($n = 0$) and normalized by the yield strength $f_{y0}t_0\,(2h_1 + 10t_0)$, for both arrangements, can be seen in Fig. 12. Both included plates as branches when η was 0.1. All models except for one failed by chord sidewall buckling or chord sidewall local yielding. One model failed due to branch effective width for all seven chord stress ratios, and was therefore excluded from the evaluation. The ultimate load $N_{1,u}$ was determined from the $3\%b_0$ deformation criterion load and the maximum load, with the maximum load governing only in cases where a peak load occurred prior to 3% deformation.

Both figures clearly show that for a bearing ratio $h_1/h_0 \leq 0.25$ no decrease, or only a negligible reduction of the connection capacity, occurs with increasing slenderness of the chord sidewall. This normalization on the vertical axis, developed by Wardenier (1982) but simplified here for 90^o branches as used in this study, assumes a dispersed width of $(h_1 + 5t_0)$ which is also the width of the equivalent steel strip or column. The model neglects the two-dimensional load-carrying effect of the chord web in which the remaining chord web gives the steel strip or column a sufficiently high stiffness such that the critical buckling stress can reach the yield stress, and thus produce connection failure by web local yielding. The experimental database also shows that, even at high chord slenderness, web yielding still occurs for small h_1/h_0 ratios, with the critical value for h_1/h_0 being around 0.2. This value is consistent with the numerical results shown.

The numerical results permit further refinement as the experimental database has limited results for small values of h_1/h_0. The equation developed by Wardenier (1982), which is based on a load dispersion slope of 1:2.5, seems to provide a very good description of the yielding behaviour. However, the web buckling behaviour must be described, which occurs in numerical tests at values of h_1/h_0 larger than 0.25. The assumption of the chord web as a pin-ended strut seems to be very conservative. Since both ends of the chord web (or strut) are relatively stiff, due to the connecting welds to the branches, fixed-fixed end conditions can be assumed for the

equivalent column. The theoretical column effective length factor K for fixed-ended struts is 0.5. In Fig. 12 the Canadian (CSA 2014) buckling curve for cold-formed RHS is plotted over the chord sidewall slenderness range. The theoretical effective length factor of K = 0.5 was used for determining χ, a reduction factor for column buckling. The "column" material properties were adopted from the tensile coupon data (which were applied for the parameter study too), where the elastic modulus was 194,000 MPa and the yield stress was 398.1 MPa. Moreover, the CSA S16-14 column curve is almost bi-linear when plotted over the complete chord sidewall slenderness range, and gives a lower bound to the numerical results.

In order to simplify the computational effort, the buckling curve can be approximated with a straight line (eq. (6)), which is only dependent on the slenderness of the chord. The buckling curve and the corresponding approximation are compared in Fig. 13. A good agreement exists over the relevant h_0/t_0 range, with the approximation erring on the conservative side.

(6) $$\chi = 1.15 - 0.013\frac{h_0}{t_0} \leq 1.0$$

Eq. (6) should ideally also be applicable for different types of steel, or yield strengths. The modulus of elasticity (E = 200,000 MPa) is constant but the yield stress term occurs in the calculation of the non-dimensional slenderness, beneath a square root. Eq. (6) can thus be modified by the term $(f_y/350)^{0.5}$, to generalize the equation.

To accommodate varying angles between the branch and the chord, the slenderness of the chord web can be increased for θ_1 <90°, with the web then considered as an equivalent slanted steel plate. For this, the term $(1/\sin\theta_1)^{0.5}$ is used since, for elastic buckling, the critical buckling stress is a function of $1/\lambda^2$. Following an elastic plate buckling study by Davies et al. (1982), Packer (1984) investigated the influence of varying branch angles on the connection ultimate strength and drew the conclusion that the term $(1/\sin\theta_1)^{0.5}$ better represented the influence of branch angle when comparing research results (albeit limited) from connections with different branch angles.

The effect of tension and compression forces in the chord on the connection capacity of welded RHS-to-RHS X-connections was examined in detail in the parametric study. The FE results, shown in Fig. 14, are grouped according to the chord sidewall slenderness, and cumulatively in the last diagram. The connection

strength in the presence of a chord axial compression or tension force ("preload"), $N_{1,u,preload}$, is plotted in a non-dimensional manner by dividing by the connection strength with zero preload (n = 0). A comparison to the existing chord stress effect reduction factors, in use by CIDECT DG3 (Q_f) and EN 1993-1-8 (k_n) for these connections, is also shown.

For the stocky specimens with a chord sidewall slenderness h_0/t_0 of 10, a large scatter of the reduction factor can be seen for tensile prestresses with the factors being approximately between 0.8 and 1.0. This can be attributed to the effect of bi-axial stress on the web yielding failure mode, which is prevalent at low wall slendernesses. Chord axial tensile stress through chord preloading, combined with transverse compressive stress due to branch loading, causes premature yielding. The failure mode of web buckling, on the other hand, is mitigated by tensile prestress because tension in the chord has a positive effect on restraining the out-of-plane deformations associated with buckling. For high compression preloading in the chord, buckling failure is initiated at an early stage, even for lower slenderness.

With increasing chord sidewall slenderness h_0/t_0, the effects of tensile and compressive prestresses become even clearer. In general, tension has a positive influence on buckling-endangered specimens (high chord sidewall slenderness h_0/t_0) and a negative influence on specimens (stocky chord) where failure is caused by local yielding. Compressive prestresses, on the other hand, have a negative effect on buckling endangered specimens (high chord sidewall slenderness h_0/t_0), as the out-of-plane bending of the chord sidewall increases with compressive loads (P-delta effect). For the stockiest chord sections, a compressive prestress causes a zero to modest drop in connection capacity. This can be ascribed to the state of bi-axial compression in the web that delays yielding, which was observed by Cheng and Becque (2016) as well.

The reduction factor for chord prestress according to EN 1993-1-8, k_n, does not consider a reduction for tensile preload in the chord. The numerical results show clear reductions for tensile prestresses in the chord of up to 0.8 (or 20% reduction), especially for specimens that fail due to local yielding. Thus, the influence function for prestress used by EN 1993-1-8 is generally unconservative for the case of tension forces in the chord. In addition, the reduction for compressive preload is limited as well and the majority of the numerical test results fall below k_n. CIDECT DG3 describes the influence of preload in the chord considerably better. A reduction for tension as well as compression in the chord is provided and the curve lies only slightly higher than results from

seven numerical tests, out of a total of 230. For the subsequent design proposal, the CIDECT DG3 chord stress reduction factor, Q_f, is adopted.

The influence of chord prestress on the connection capacity for plate-to-RHS X-connections was investigated separately to RHS-to-RHS X-connections, because a different reduction factor, Q_f, is proposed for plate-to-RHS connections by CIDECT DG3. The reduction factor for tensile preload remains the same, but the compressive preloading effect is potentially more severe, depending on the chord sidewall slenderness h_0/t_0. The value C_1 is 0.03γ (Wardenier et al. 2010), where $C_1 \geq 0.1$. The value of $k_n = 1.0$ is used by EN 1993-1-8 for transverse plate-to-RHS connections. Following the same approach as for RHS-to-RHS X-connections, the numerical ultimate strengths were divided by the corresponding connection results without preload (n = 0). Numerical results for chord sidewall slenderness values h_0/t_0 of 10, 20 and 30 are plotted collectively in Fig. 15 since the data for plate-to-RHS connections are limited. Chord sidewall slenderness values > 40, or exceeding Class 2 cross sections, exceed the CIDECT DG3 range of validity and only tensile prestresses were examined.

The capacity of plate-to-RHS X-connections, which all fail by web yielding, is mainly influenced by compressive prestresses in the chord, which was observed by Lu (1997) as well. For this case, reductions of up to 0.8 (or 20% reduction) occur, whereas tensile forces in the chord generally have a lower influence on the connection capacity. For stress ratios n between 0 and 1, k_n is generally unconservative and Q_f is almost a lower bound. For negative stress ratios (compressive preloading), k_n is always unsafe but Q_f gives a reasonably good influence function. The need for a different Q_f reduction factor, dependent on the chord web slenderness h_0/t_0, is not apparent from the numerical results and $C_1 = 0.1$ (in eq. (2)) is adequate.

Evaluation of Results for Design

The identified trends and influences are now brought together and transferred into a new or modified design model. For this purpose, the RHS sidewalls are treated as short columns or struts, for all geometric arrangements, which is the design approach used by CIDECT DG3 (Packer et al. 2009), EN 1993-1-8 (CEN 2005) and the CISC Design Guide (Packer and Henderson 1997).

The connection behaviour of RHS-to-RHS X-connections is strongly dependent on two parameters: the chord sidewall slenderness and the bearing length to chord height ratio, $(h_1/\sin\theta_1)/\ h_0$. Therefore, these

parameters must be represented in the design model. The existing CIDECT DG3 design method predicts buckling failure for connections with $h_0/t_0 > 10$, which includes almost all connections as well as stocky chords where yielding failure governs, and thus gives substantially lower strength for these connections. Even for connections where CIDECT DG3 correctly predicts a "buckling" failure, the assumption of a pin-ended strut still leads to conservative estimates. Hence, the CIDECT DG3 approach could be modified to:

- Distinguish between web buckling and yielding failure, according to geometric parameters above and below the critical value for h_1/h_0 of 0.25
- Compute the buckling reduction factor χ assuming fixed-fixed end conditions for welded connections, fixed-pinned end conditions for connections welded on one side, and pinned-pinned end condition for unwelded connections
- Approximate the buckling stress factor χ as a function of $(h_0 - 2t_0)/t_0$ (Fig. 16), and additionally use $1/(\sin\theta_1)^{0.5}$ to take into account the higher chord web slenderness with inclined branches.

The proposed changes are summarized as follows. The nominal connection strength is given by:

$$N_1 = 2\chi f_{y0} t_0 \left(\frac{h_1}{\sin\theta_1} + 5t_0\right) Q_f \quad (7)$$

where, for $h_1/h_0 \leq 0.25$, $\chi = 1.0$ (yielding) and h_1 is the branch depth. For X-connections welded on one side, $h_1/\sin\theta_1$ is the minimum of the bearing lengths on the two sides of the chord. The buckling factor χ, can be calculated from a wall slenderness, λ, according to CSA S16-14 using the cold-formed buckling curve, with the design value effective length factors from the informative Annex F:

- $\lambda = K \cdot 3.46\left(\frac{h_0}{t_0} - 2\right)\sqrt{\frac{1}{\sin\theta_1}}$ (when both branches/plates are welded to the chord, using $K_{CSA} = 0.65$)
- $\lambda = K \cdot 3.46\left(\frac{h_0}{t_0} - 2\right)\sqrt{\frac{1}{\sin\theta_1}}$ (when one branch/plate is welded to the chord and the other is unwelded, using $K_{CSA} = 0.80$)
- $\lambda = K \cdot 3.46\left(\frac{h_0 + b_0}{2t_0} - 2\right)\sqrt{\frac{1}{\sin\theta_1}}$ (when both branches/plates are unwelded, using $K_{CSA} = 1.0$)

As an alternative, the buckling factor χ can also be approximated with a straight line and generally expressed so that different steel strengths can also be used. However, this is only possible for fixed-fixed end

conditions, otherwise the buckling curve plotted over the h_0/t_0 range is not linear. The function for χ, given by eq. (8), a generalized version of eq. (6), is directly related to the chord sidewall slenderness and allows for a very fast, uncomplicated and precise alternative to the complex calculation of the factor χ, which in turn requires calculation of a column slenderness ratio λ.

(8) $$\chi = 1.15 - 0.013\frac{h_0}{t_0}\sqrt{\frac{1}{sin\theta_1}}\sqrt{\frac{f_y}{350}} \leq 1$$

In the following assessment, the approximate function (eq. (8)) is used for the case of both branches being welded. If determining χ from λ it is recommended that the cold-formed buckling curve always be used, for hot-formed, cold-formed stress-relieved (Class H), and cold-formed (Class C) RHS. This makes it easier for routine engineering and it is safe, if there is indeed an advantage for using hot-formed or Class H RHS. At present EN 1993-1-8 refers to use of the "relevant" buckling curve, which is confusing and may possibly lead to unsafe design. In addition, it can be noted that the "hot" and "cold" buckling curves represent global failure of columns, whereas the bulging of an RHS sidewall is a local failure. To describe the influence of chord prestress, the CIDECT DG3 factor Q_f, eq. (2), is adopted, for both RHS-to-RHS and plate-to-RHS full-width ($\beta = 1$) connections, as this formula has provided a very good estimation of the behaviour.

Welded X-connections: RHS-to-RHS and plate-to-RHS

In this section an evaluation is made of the proposed design method, represented by eq. (7) and eq. (8), against both numerical and experimental results. Ultimate strengths r_t and r_e are used in the correlation, where r_t represents the connection theoretical capacity according to the design model, and r_e represents the experimental (as well as the numerical) connection test capacity. There is no difference between plate-to-RHS connections and RHS-to-RHS connections if h_1/h_0 is less than 0.25. Thus, a general formulation is achieved, which is differentiated according to the type of failure (yielding or buckling). The only small difference is that h_1 in eq. (7) needs to be replaced by t_1 for plate branches. Figs. 17 to 22 show the correlation between actual (numerical or experimental tests results) and predicted connection strengths. A simplified reliability analysis has also been performed, using North American procedures (Fisher at al. 1978; Ravindra and Galambos 1978) with a target

safety index of 3.0 for ductile connections. The resulting resistance factors, ϕ, along with statistical measures of fit, are shown in the figures.

All numerical data with chord sections classified as Class 1 or 2 were included in the correlations, with the chord prestressed under either compression and tension within the range $-0.75 \leq n \leq 0.75$. (Numerical results with chord sidewall slenderness h_0/t_0 of 40 and 50 are class 4). A good correlation is shown with numerical tests for RHS-to-RHS (Fig. 17) and plate-to-RHS (Fig. 18) connections, with a low coefficient of variation (COV) of 0.09 for both cases. In addition, actual-to-predicted mean values of 1.22 and 1.28 represent a very economical and accurate statement for the connection capacity.

Likewise, all experimental results from the connection database (in Table 8) are similarly compared to the theoretical model in Figs. 19 and 20. All 51 results of the "welded" RHS-to-RHS and 25 of the plate-to-RHS connections were compared to get the best possible indication of the safety level, even though some were not in the range of validity of CIDECT DG3 and covered Class 1 to Class 4 RHS. Again, a reasonable correlation between the proposed model and the experimental results can be seen in Figs. 19 and 20. The COVs are larger than for the numerical results, which is expected when using data from diverse international sources.

In addition, just experimental results falling within the CIDECT DG3 parameter range of validity have been assessed separately, to particularly justify design recommendations within a parameter range. Only 31 tests for RHS-to-RHS and 8 tests for plate-to-RHS connections meet these constraints, because many had chord sections which were class 3 or 4 (probably to ensure failure by chord sidewall buckling). By excluding the very slender chord sidewall tests due to the CIDECT DG3 range of validity, a better correlation can be obtained between the prediction model and relevant experiments (Figs. 21 and 22). Overall, the evaluations support a resistance factor ϕ of 1.0 for the case of Class 1 and 2 RHS-to-RHS connections (see Figs. 17, 19 and 21), and in excess of 1.0 for plate-to-RHS connections (see Figs. 18, 20 and 22), which is ideal for application to CSA S16. The new design proposal thus provides a much better formulation of the connection capacity and predicts the actual connection behaviour much better.

Welded on one side and unwelded X-connections: RHS-to-RHS and plate-to-RHS

The evaluation of X-connections welded on both sides has been carried out in great detail, since this is the prime focus of this paper. However, an additional 28 experimental tests with a branch welded on one side (in Table 9), and 20 experimental tests with unwelded branches (in Table 10), are available for evaluation against the proposed design procedure, with results shown in Table 7.

With the conservative assumption of taking the smaller value of the two bearing lengths, an acceptable safety level can be achieved for "welded on one side" connections. The COV is tolerable in conjunction with the high mean. The mean value of approximately 1.5 indicates a prediction model that is very conservative and has much room for improvement. For "unwelded" connections the implied resistance factor of 0.74 is unacceptably low and further study is necessary.

Conclusions

A numerical parametric study of full-width ($\beta = 1.0$), welded RHS X-connections is presented, with the finite element models used being validated against carefully performed connection tests in the laboratory. In addition, a large database of additional international experiments on related connections has been assembled.

Preliminary finite element modelling illustrated a significant difference in connection capacity between different experimental testing arrangements, which was also found in the experimental database (consisting of a total of 125 tests). Accordingly, RHS X-connections were classified into three different categories depending on the attachment of their branches or bearing plates: "welded" (fixed-fixed web restraint), "welded on one side" (fixed-pinned web restraint), and "unwelded" (pinned-pinned web restraint).

The non-linear numerical parametric study included 350 models, covering a wide range of dimensionless geometric variables, and investigated the influence of compressive and tensile stress in the chord on the connection capacity. Determination of the connection capacity included consideration of a 3% chord face deformation limit.

In general, a reduction of the connection capacity was evident for both compression and tension stress in the chord, relative to zero chord stress. The reductions for different levels of chord preloading (up to 75% of the

yield stress) were captured very well by the current Q_f formula in CIDECT Design Guide No. 3 (Packer at al. 2009), which is a conservative approximation of the Q_f for K-connections.

The main influence on the connection behaviour could be attributed to the chord sidewall slenderness ratio and the ratio of bearing length to chord height, $(h_1/\sin\theta_1)/h_0$. A critical value of 0.25 for the $(h_1/\sin\theta_1)/h_0$ ratio was established, at which a transition from a failure mode of web yielding to web buckling takes place, allowing a common method for handling RHS-to-RHS X-connections with $(h_1/\sin\theta_1)/h_0 \leq 0.25$ and plate-to-RHS connections. The proposed nominal connection strength is given by:

$$N_1 = 2\chi f_{y0} t_0 \left(\frac{h_1}{sin\theta_1} + 5t_0\right) Q_f$$

- For $(h_1/\sin\theta_1)/h_0 \leq 0.25$, $\chi = 1.0$ (web yielding failure mode) and h_1 is the RHS branch depth (or branch plate thickness). For X-connections welded on one side, h_1 is the minimum of the bearing lengths on either side of the chord. For fully-welded, or welded on one side connections, the factored resistance (N_1^*) can be obtained by the inclusion of a resistance factor (ϕ) of 1.0; for unwelded branches $\phi = 0.7$.
- For $(h_1/\sin\theta_1)/h_0 > 0.25$, $\chi \leq 1.0$ (web buckling failure mode) and χ is calculated from the chord sidewall slenderness, λ, using the CSA S16 cold-formed buckling curve, where:

$$\lambda = K \cdot 3.46\left(\frac{h_0}{t_0} - 2\right)\sqrt{\frac{1}{sin\,\theta_1}}$$ for both branches "welded", with $K_{CSA} = 0.65$ and $\phi = 1.0$

$$\lambda = K \cdot 3.46\left(\frac{h_0}{t_0} - 2\right)\sqrt{\frac{1}{sin\,\theta_1}}$$ for one branch"welded on one side", with $K_{CSA} = 0.80$ and $\phi = 1.0$

$$\lambda = K \cdot 3.46\left(\frac{h_0 + b_0}{2t_0} - 2\right)\sqrt{\frac{1}{sin\,\theta_1}}$$ for both branches unwelded, with $K_{CSA} = 1.0$ and $\phi = 0.7$

and

$Q_f = (1 - |n|)^{C_1}$ with $C_1 = 0.1$.

The parameter limits of validity for the empirical design recommendation are:

(i) Cross-section slenderness: Class 1 and 2 sections for RHS chord;

(ii) Bearing length: $(h_1/\sin\theta_1)/h_0$ or $t_1/h_0 \leq 2.0$

(iii) RHS chord aspect ratio: $0.5 \leq h_0/b_0 \leq 2.0$

(iv) Branch angle: $\theta_1 \geq 45^o$ for RHS branches; $\theta_1 \approx 90^o$ for plate branches;

(v) Material: $f_{y1} \leq f_{y0}$; $f_y \leq 0.8f_u$; $f_y \leq 460$ MPa.

(vi) Chord preload: $-0.75 \leq n \leq 0.75$

For fully welded X-connections, and assuming fixed-fixed end conditions ($K_{CSA} = 0.65$), the CSA S16 cold-formed RHS buckling curve is almost linear when plotted over the practical chord sidewall slenderness range. Therefore, an approximation given by eq. (8) may be used to determine χ when $(h_1/\sin\theta_1)/h_0 > 0.25$, in lieu of the λ method above.

For unwelded X-connections, and assuming pinned-pinned end conditions ($K_{CSA} = 1.0$), the low resistance factor ($\phi = 0.7$) associated with the web buckling model is indicative of a need for further research.

This new design approach for RHS sidewalls under transverse compression strongly outperforms the current (very conservative) CIDECT DG3 model for chord sidewall failure under transverse compression, and is considerably more accurate than the current (often unsafe) recommendations given by CSA S16-14 and AISC 360-16.

Acknowledgements

The authors are grateful for the financial support provided by the Canadian Institute of Steel Construction (CISC) and the Natural Sciences and Engineering Research Council of Canada (NSERC), as well as the in-kind donation of RHS materials by Atlas Tube Inc. The collaboration of Professor T. Ummenhofer, Karlsruhe Institute of Technology, Germany, and Prof. K. Tousignant, Dalhousie University, is also gratefully acknowledged, as is the laboratory assistance of Mr. F. Wei.

References

AISC. 2016. Specification for structural steel buildings. ANSI/AISC 360-16, American Institute of Steel Construction, Chicago, USA.

Boresi, A. P., and Schmidt, R. J. 2003. Advanced mechanics of materials, 6th ed., John Wiley & Sons. Inc., New Jersey, USA.

CEN. 2005. Eurocode 3: Design of steel structures – Part 1-8: Design of joints. EN 1993-1-8:2005+AC:2009, European Committee for Standardization, Brussels, Belgium.

Cheng, S., and Becque, J. 2016. A design methodology for side wall failure of RHS truss X-joints accounting for compressive chord pre-load. Engineering Structures, **126**: 689–702.

CSA. 2014. Design of steel structures. CSA S16-14, Canadian Standards Association, Toronto, Canada.

Davies, G., and Packer, J.A. 1987. Analysis of web crippling in a rectangular hollow section. Proceedings of the Institution of Civil Engineers, Part 2, **83**: 785–798.

Davies, G., Platt, J.C., and Snell, C. 1982. The buckling of long simply supported rectangular plates under partially distributed skew pinch loads. Report NUCE/ST/10-1982, Department of Civil Engineering, University of Nottingham, Nottingham, U.K.

Fan, Y. 2017. RHS-to-RHS axially loaded X-connections offset towards an open chord end. MASc thesis, University of Toronto, Toronto, Canada.

Fisher, J.W., Galambos, T.V., Kulak, G.L., and Ravindra, M.K. 1978. Load and resistance factor design criteria for connectors. Journal of the Structural Division, American Society of Civil Engineers, **104**(9): 1427–1441.

ISO. 2013. Static design procedure for welded hollow section joints – Recommendations. ISO 14346, International Organization for Standardization, Geneva, Switzerland.

Lipp, A., and Ummenhofer, T. 2014. Influence of tensile chord stresses on the strength of circular hollow section joints. Steel Construction, **7**(2): 126–132.

Lu, L. H. 1997. The static strength of I-beam to rectangular hollow section column sections. PhD thesis, Delft University of Technology, Delft, The Netherlands.

Lu, L.H., de Winkel, G.D., Yu, Y., and Wardenier, J. 1994. Deformation limit for the ultimate strength of hollow section joints. *In* Proceedings of the 6th International Symposium on Tubular Structures, Melbourne, Australia, pp. 341–347.

Packer, J. A. 1984. Web crippling of rectangular hollow sections. Journal of Structural Engineering, American Society of Civil Engineers, **110**(10): 2357– 2373.

Packer, J.A. 1987. Review of American RHS web crippling provisions. Journal of Structural Engineering, American Society of Civil Engineers, **113**(12): 2508–2513.

Packer, J. A., and Henderson, J.E. 1997. Hollow structural section connections and trusses – A design guide, 2nd ed. Canadian Institute of Steel Construction, Toronto, Canada.

Packer, J.A., Puthli, R., van der Vegte, G.J., and Wardenier, J. 2017. Discussion on the paper "Experimental and numerical assessment of RHS T-joints subjected to brace and chord axial forces", by Nizer et al., in **9**(4), 2016, Steel Construction, **10**(1): 89–90.

Packer, J. A., Wardenier, J., Zhao, X.-L., van der Vegte, G. J., and Kurobane, Y. 2009. Design guide for rectangular hollow section (RHS) joints under predominantly static loading. CIDECT Design Guide No. 3, 2nd ed. CIDECT, Geneva, Switzerland.

Poloni, T. 1985. The effect of bearing length on transversely compressed RHS. BASc thesis, University of Toronto, Toronto, Canada.

Ravindra, M.K., and Galambos, T.V. 1978. Load and resistance factor design for steel. Journal of the Structural Division, American Society of Civil Engineers, **104**(9): 1337–1353.

Serrano, M.A., Lopez-Colina, C., Lozano, M., and Iglesias, G. 2017. CUVIPIMECO characterisation of I-beam to RHS-column joints, CIDECT Report 5CE, University of Oviedo, Gijon, Spain.

Swanson Analysis Systems. 2017. ANSYS ver. 18.0. Houston, USA.

van der Vegte, G.J., Wardenier, J., and Puthli, R.S. 2010. FE analysis for welded hollow-section joints and bolted joints. Structures and Buildings, Proceedings of the Institution of Civil Engineers, **163**(6): 427–437.

Voth, A. P., and Packer, J. A. 2012. Numerical study and design of T-type branch plate-to-circular hollow section connections. Engineering Structures, **41**: 477–489.

Wardenier, J. 1982. Hollow section joints. Delft University of Technology, Delft, The Netherlands.

Wardenier, J., Packer, J.A., and Puthli, R. 2018. Simplified design equations for plate-to-CHS T and X joints for use in codes. Steel Construction, **11**(2): 146–161.

Wardenier, J., Packer, J.A., Zhao, X.-L., and van der Vegte, G.J. 2010. Hollow sections in structural applications, 2nd ed. CIDECT, Geneva, Switzerland.

Wardenier, J., van der Vegte, G.J. and Liu, D.K. 2007. Chord stress function for rectangular hollow section X and T joints. *In* Proceedings of the International Offshore and Polar Engineering Conference, Lisbon, Portugal, Vol. IV, pp. 3363–3370.

Zhao, X.-L., and Hancock, G. J. 1992. Square and rectangular hollow sections subject to combined actions. Journal of Structural Engineering, American Society of Civil Engineers, **118**(3): 648–667.

List of Symbols

a_w throat thickness of weld (mm)

b_0 external width of RHS chord (mm)

b_1 external width of RHS branch (mm)

E modulus of elasticity (MPa)

f_b buckling stress, using column slenderness ratio λ per EN 1993-1-8 (MPa)

f_k buckling stress, using column slenderness ratio λ per CIDECT DG3 (MPa)

f_u ultimate stress (MPa)

f_y yield stress (MPa)

f_{y0} yield stress of chord (MPa)

f_0 compression stress in chord connecting face (MPa)

h_0 external height of RHS chord (mm)

h_1 external height of RHS branch (mm)

k_n chord stress factor to account for the effect of chord normal stress in the chord connecting face per EN 1993-1-8

K column or strut effective length factor; KL = effective length (mm)

l_i branch length (mm)

l_0 chord length (mm)

n chord member stress ratio = normal stress in the chord divided by the chord yield load (compression negative; tension positive); parameter for column buckling in CSA S16

N_1 branch axial force (N)

$N_{1,max}$ maximum connection load (N)

$N_{1,u}$ ultimate connection load, without chord preload (N)

$N_{1,u,preload}$ ultimate connection load, with chord preload (N)

N_1^* connection factored resistance (N)

$N_{1,Rk}$ connection design resistance in EN 1993-1-8 (N)

$N_{1,3\%}$ connection load at a deformation of $3\%b_0$ (N)

Q_f chord stress factor to account for the effect of chord normal stress in the chord connecting face per CIDECT DG3, AISC 360 and ISO 14346.

r_e connection strength from experimental or numerical tests (N)

r_i inside corner radius of RHS (mm)

r_o outside corner radius of RHS (mm)

r_t connection strength predicted by theoretical model (N)

t_0 wall thickness of RHS chord (mm)

t_1 wall thickness of RHS branch or thickness of plate (mm)

β branch-to-chord width ratio (= b_1/b_0 for RHS branch)

2γ width-to-thickness ratio of RHS chord = b_0/t_0

γ_{M5} partial safety factor in EN 1993-1-8 (=1.0 for buildings)

ε engineering strain

ε_T true strain

ε_y strain at yield

ε_{rup} strain at rupture

η branch height-to-chord width ratio = h_1/b_0 or t_1/b_0

θ_1 included angle between branch and chord (^{o})

λ slenderness of a column/strut or chord sidewall

σ engineering stress (MPa)

σ_T true stress (MPa)

τ branch-to-chord thickness ratio = t_1/t_0

ϕ resistance factor in CSA S16 or AISC 360

χ reduction factor applied to yield stress for column buckling

List of Figure Captions

Fig. 1. Notation for RHS-to-RHS X-connections

Fig. 2. Notation for transverse plate-to-RHS X-connections

Fig. 3. Comparison of different reduction factors to account for chord stress

Fig. 4. Different testing arrangements for full-width RHS connections: (a) welded to both branches: "welded"; (b) unwelded; (c) welded to one branch and pushed against a rigid base: "welded on one side"

Fig. 5. Typical testing arrangement for full-width test specimens, with failure by web buckling

Fig. 6. Connection load-displacement curves, for: (a) RHS chord with $2\gamma = 21$ (X2); (b) RHS chord with $2\gamma = 32$ (X1)

Fig. 7. One-eighth model used for RHS-to-RHS welded X-connections

Fig. 8. Engineering stress-strain curves for 3 tensile coupon tests, and true stress-strain curve from the average

Fig. 9. FE meshing options examined for RHS-to-RHS connections: (a) fine; (b) coarse; (c) medium

Fig. 10. Experimental vs. FE load-displacement curves for: (a) RHS chord with $2\gamma = 21$ (X2); (b) RHS chord with $2\gamma = 32$ (X1)

Fig. 11. Comparison of experimental and numerical chord sidewall deformations (specimen X1): (a) X1, connection failure mode, for $\delta_v \approx 20$ mm; (b) X1, von Mises nodal stresses, for $\delta_v \approx 8$ mm

Fig. 12. Normalized FE connection strengths, with $n = 0$, for: (a) square chord; (b) rectangular chord

Fig. 13. CSA S16 buckling curve for cold-formed RHS and a linear approximation, for $f_y = 350$ MPa

Fig. 14. Effect of chord stress on RHS-to-RHS X-connections and comparison with existing reduction factors

Fig. 15. Effect of chord preloading on the strength of plate-to-RHS X-connections

Fig. 16. Modified chord wall yielding/buckling model with 1:2.5 load dispersion

Fig. 17. Statistical evaluation of 152 numerical tests for chord web failure of RHS-to-RHS X-connections, with Class 1 and 2 RHS chords

Fig. 18. Statistical evaluation of 49 numerical tests for chord web failure of plate-to-RHS X-connections, with Class 1 and 2 RHS chords

Fig. 19. Statistical evaluation of 51 experimental tests (Table 8) for chord web failure of RHS-to-RHS X-connections, for all classes of RHS chord

Fig. 20. Statistical evaluation of 25 experimental tests (Table 8) for chord web failure of plate-to-RHS X-connections, for all classes of RHS chord

Fig. 21. Statistical evaluation of 31 experimental tests (Table 8) for chord web failure of RHS-to-RHS X-

connections, within the CIDECT parameter range of validity and Class 1 and 2 RHS chords

Fig. 22. Statistical evaluation of 8 experimental tests (Table 8) for chord web failure of plate-to-RHS X-connections, within the CIDECT parameter range of validity and Class 1 and 2 RHS chords

Table 1. Summary of design recommendations for RHS web compression, applied to full-width X-connections

Design Code	Limit state	Factored Connection Strength	ϕ or γ_{M5} factor
CSA S16-14	yielding	$N_1^* = \frac{2f_{y0}t_0}{sin\theta_1}\left(\frac{h_1}{sin\theta_1} + 10t_0\right)\phi$	0.80
	buckling	$N_1^* = \frac{1280t_0\left(\frac{h_1}{sin\theta_1} + 10t_0\right)}{sin\theta_1(h_0/t_0 - 3)^2}Q_f\phi$	0.80
	crippling	$N_1^* = \frac{2.9t_0^2}{sin\theta_1}\sqrt{Ef_{y0}}Q_f\phi$	0.80
AISC 360-16	yielding	$N_1^* = \frac{2f_{y0}t_0}{sin\theta_1}\left(\frac{h_1}{sin\theta_1} + 7.5t_0\right)\phi$	1.00
	buckling	$N_1^* = \frac{1}{sin\theta_1}\left(\frac{48t_0^3}{h_0 - 3t_0}\right)\sqrt{Ef_{y0}}Q_f\phi$	0.90
Eurocode 3	yielding/ buckling	$N_{1,Rk} = \frac{2f_bt_0}{sin\theta_1}\left(\frac{h_1}{sin\theta_1} + 5t_0\right)k_n/\gamma_{M5}$	1.00
CIDECT/ISO	yielding/ buckling	$N_1^* = \frac{2f_kt_0}{sin\theta_1}\left(\frac{h_1}{sin\theta_1} + 5t_0\right)Q_f$	Included

Table 2. Test specimen identification and measured geometric variables

Specimen	Width ratio β	Chord slenderness 2γ	Wall-thickness ratio τ	Chord length l_0 [mm]	Branch lengths l_i [mm]	Weld size a_w [mm]
X1	1.0	32	1.96	1603	808	6.8
X2	1.0	21	1.32	1303	808	6.9

Table 3. Measured RHS dimensions

Nominal dimensions [mm]	Member	Height h [mm]	Width b [mm]	Wall-thickness t [mm]	Corner radii Outer r_o [mm]	Corner radii Inner r_i [mm]
RHS 203x203x6.35	Chord	203.6	203.6	5.96	14.98	8.99
RHS 203x203x9.53	Chord	203.1	203.1	8.85	23.82	14.98
RHS 203x203x12.7	Branch	204.0	204.0	11.67	32.67	21.04

Table 4. Average measured RHS chord mechanical properties

Designation [mm]	E [MPa]	f_y [MPa]	ε_y	f_u [MPa]	ε_{rup}	f_y/f_u
RHS 203x203x6.35	197400	388.8	0.00401	508.7	0.287	0.76
RHS 203x203x9.53	194000	398.1	0.00405	519.8	0.306	0.77

Table 5. FE sensitivity study for specimen X2

Element type	No. of elements	No. of nodes	μ	thickness elements	Mesh type	$N_{1,exp.}$ [kN]	$N_{1,}$ $[kN]_{FE}$	$\frac{N_{1,exp}}{N_{1,FE}}$
SOLID185	85 851	100 978	0.1	4	Coarse		1277	0.99
SOLID185	**85 851**	**100 978**	**0.3**	**4**	**Coarse**		**1310**	**0.96**
SOLID185	85 851	100 978	0.5	4	Coarse		1334	0.95
SOLID185	85 851	100 978	0.7	4	Coarse		1349	0.94
SOLID185	31 819	39 960	0.3	3	Coarse		1275	0.99
SOLID185	54 256	66 172	0.3	3	Medium	1264	1274	0.99
SOLID185	104 131	126 360	0.3	3	Fine		1274	0.99
SOLID185	10 509	14 196	0.3	2	Coarse		1217	1.04
SOLID185	169 404	193 181	0.3	5	Coarse		1322	0.96
SOLID186	10509	47 178	0.3	2	Coarse		1328	0.95
SOLID186	41 259	183 281	0.3	3	Coarse		1338	0.95

Table 6. FE sensitivity study for specimen X1

Element type	No. of elements	No. of nodes	μ	thickness elements	Mesh type	$N_{1,exp.}$ [kN]	$N_{1,FE}$ [kN]	$\frac{N_{1,exp}}{N_{1,FE}}$
SOLID185	144 354	173 581	0.1	4	Coarse		630	1.04
SOLID185	**144 354**	**173 581**	**0.3**	**4**	**Coarse**		**649**	**1.00**
SOLID185	144 354	173 581	0.5	4	Coarse		662	0.99
SOLID185	144 354	173 581	0.7	4	Coarse		672	0.97
SOLID185	64 017	80 803	0.3	3	Coarse		633	1.03
SOLID185	117 085	142 445	0.3	3	Medium	653	632	1.03
SOLID185	172 336	216 379	0.3	3	Fine		633	1.03
SOLID185	21 273	28 994	0.3	2	Coarse		594	1.10
SOLID185	-	-	0.3	5	Coarse		-	-
SOLID186	21 273	101 479	0.3	2	Coarse		664	0.98
SOLID186	64 017	297 549	0.3	3	Coarse		666	0.98

Table 7. Correlation between experimental tests and the proposed design method, for full-width unwelded and welded on one side RHS connections

Type of web restraint	r_e/r_t (ultimate strength)			
	No. of tests	Mean	COV	ϕ
Welded on one side; prediction using K_{CSA} = 0.80 and eq. (7)	28	1.49	0.23	1.02
Unwelded; prediction using K_{CSA} = 1.0 and eq. (7)	20	1.08	0.23	0.74

Table 8. 77 Tests on Full-Width, Compression-Loaded, RHS X-connections, with Welded Branches

Researcher / year	Location	Specimen no.	b_0 x h_0 x t_0 [mm]	A_0 [mm^2]	b_1 x h_1 x t_1 [mm][1,2]	θ_1 [^{0}][2]	f_{y0} [MPa][3]	f_0 [MPa][4]	N_{1u} [kN]	Forming process[5]	Failure mode
Dixon/83	Toronto	D1121	101.7 x 77.6 x 5.08	1649	101.7 x 77.6 x 5.08	90	300.7	0	403	HF	Buckling
Dixon/83	Toronto	D1122	77.8 x 101.8 x 4.93	1571	77.8 x 101.8 x 4.93	90	370.3	0	445	HF	Buckling
Dixon/83	Toronto	D1222	77.8 x 101.8 x 4.93	1571	77.8 x 101.8 x 4.93	45	370.3	0	476	HF	Buckling
Dixon/83	Toronto	D1322	77.8 x 101.8 x 4.93	1571	77.8 x 101.8 x 4.93	60	370.3	0	459	HF	Buckling
Dixon/83	Toronto	D2121	304.4 x 204.1 x 7.21	6884	304.4 x 204.1 x 7.21	90	406.3	0	1315	CFSR	Buckling
Dixon/83	Toronto	D2122	204.1 x 304.4 x 7.21	6884	204.1 x 304.4 x 7.21	90	406.3	0	1230	CFSR	Buckling
Dixon/83	Toronto	D2212	204.1 x 304.4 x 7.21	6884	203.4 x 25.94 x 25.94	45	406.3	0	700	CFSR	Bearing
Dixon/83	Toronto	D2222	204.1 x 304.4 x 7.21	6884	204.1 x 304.4 x 7.21	45	406.3	0	1675	CFSR	Buckling
Dixon/83	Toronto	D3121	203.2 x 153.6 x 4.83	3231	203.2 x 153.6 x 4.83	90	391.6	0	649	CFSR	Buckling
Dixon/83	Toronto	D3122	153.6 x 203.2 x 4.83	3231	153.6 x 203.2 x 4.83	90	411.5	0	530	CFSR	Buckling
Dixon/83	Toronto	D3221	203.2 x 153.6 x 4.83	3231	203.2 x 153.6 x 4.83	44	391.6	0	693	CFSR	Buckling
Dixon/83	Toronto	D3222	153.6 x 203.2 x 4.83	3231	153.6 x 203.2 x 4.83	44	411.5	0	694	CFSR	Buckling
Dixon/83	Toronto	D4123	254.1 x 254.1 x 9.35	8795	254.1 x 254.1 x 9.35	90	405.5	0	2183	CFSR	Buckling
Dixon/83	Toronto	D4223	254.1 x 254.1 x 9.35	8795	254.1 x 254.1 x 9.35	45	405.5	0	2429	CFSR	Buckling
Dixon/83	Toronto	D4323	254.1 x 254.1 x 9.35	8795	254.1 x 254.1 x 9.35	60	405.5	0	2215	CFSR	Buckling
Dixon/82	Toronto	DD11	77.6 x 101.7 x 5.08	1649	78.9 x 12.62 x 12.62	90	300.7	0	180	HF	Bearing
Dixon/82	Toronto	DD12	101.7 x 77.6 x 5.08	1649	104.4 x 12.62 x 12.62	90	300.7	0	210	HF	Bearing
Dixon/82	Toronto	DD13	77.6 x 101.7 x 5.08	1649	78.7 x 12.62 x 12.62	60	300.7	0	200	HF	Bearing
Dixon/82	Toronto	DD14	101.7 x 77.6 x 5.08	1649	102.1 x 12.62 x 12.62	58	300.7	0	204	HF	Bearing
Dixon/82	Toronto	DD31	204.1 x 304.4 x 7.21	6884	205.9 x 20.32 x 20.32	90	406.3	0	501	CFSR	Bearing
Dixon/82	Toronto	DD32	304.4 x 204.1 x 7.21	6884	303.8 x 20.32 x 20.32	90	406.3	0	462	CFSR	Bearing
Dixon/82	Toronto	DD33	204.1 x 304.4 x 7.21	6884	204.7 x 20.32 x 20.32	59	406.3	0	566	CFSR	Bearing
Dixon/82	Toronto	DD34	304.4 x 204.1 x 7.21	6884	304.9 x 20.32 x 20.32	60	406.3	0	547	CFSR	Bearing

Table 8. 77 Tests on Full-Width, Compression-Loaded, RHS X-connections, with Welded Branches

Researcher / year	Location	Specimen no.	b_0 x h_0 x t_0 [mm]	A_0 [mm^2]	b_1 x h_1 x t_1 [mm][1,2]	θ_1 [°][2]	f_{y0} [MPa][3]	f_0 [MPa][4]	N_{1u} [kN]	Forming process[5]	Failure mode
Erdosy/81	Toronto	A1	177.6 x 127.8 x 4.74	2849	175.8 x 13.34 x 13.34	90	335.5	0	200	CFSR	Bearing
Erdosy/81	Toronto	A2	177.6 x 127.8 x 4.74	2849	176.2 x 12.61 x 12.61	90	335.5	63.7	190	CFSR	Bearing
Erdosy/81	Toronto	A3	177.6 x 127.8 x 4.74	2849	176.1 x 12.61 x 12.61	90	335.5	124.1	160	CFSR	Bearing
Erdosy/81	Toronto	A4	177.6 x 127.8 x 4.74	2849	176 x 12.61 x 12.61	90	335.5	151.0	171	CFSR	Bearing
Erdosy/81	Toronto	B1	127.4 x 177.4 x 4.82	2880	125.3 x 12.61 x 12.61	90	336.0	0	194	CFSR	Bearing
Erdosy/81	Toronto	B2	127.4 x 177.4 x 4.82	2880	125.4 x 12.61 x 12.61	90	336.0	60.5	197	CFSR	Bearing
Erdosy/81	Toronto	B3	127.4 x 177.4 x 4.82	2880	125.5 x 12.61 x 12.61	90	336.0	127.7	176	CFSR	Bearing
Erdosy/81	Toronto	B4	127.4 x 177.4 x 4.82	2880	125.4 x 12.61 x 12.61	90	336.0	147.8	184	CFSR	Bearing
Davies/82	Nottingham	X(1)PR90	100 x 100 x 4.04	1551	100 x 22.2	90	320.0	0	183	HF	Buckling
Davies/82	Nottingham	X(2)PR45	100 x 100 x 4.04	1551	100 x 22.2	45	320.0	0	252	HF	Buckling
Davies/82	Nottingham	X(3)RR90	100 x 100 x 3.97	1525	100 x 100 x 4	90	320.0	0	353	HF	Buckling
Davies/82	Nottingham	X(4)RR45	100 x 100 x 3.95	1525	100 x 100 x 4	45	320.0	0	372	HF	Buckling
Platt/82	Nottingham	X-RR-90-A	100 x 100.2 x 4.2	1604	100 x 100 x 4	90	432.0	0	391	CF	Buckling
Platt/82	Nottingham	X-RR-60-A	99.8 x 100.1 x 4.2	1594	100 x 100 x 4	60	432.0	0	410	CF	Buckling
Platt/82	Nottingham	X-RR-45-A	100.1 x 100 x 4.2	1599	100 x 100 x 4	45	432.0	0	450	CF	Buckling
Platt/82	Nottingham	X-RR-90-B	98.7 x 100 x 4	1529	100 x 50 x 5	90	311.0	0	209	HF	Buckling
Platt/82	Nottingham	X-RR-60-B	98.9 x 100 x 4.1	1556	100 x 50 x 5	60	311.0	0	218	HF	Buckling
Platt/82	Nottingham	X-RR-45-B	99.2 x 100 x 4	1544	100 x 50 x 5	45	311.0	0	244	HF	Buckling
Platt/82	Nottingham	X-RR-90-C	250 x 251.1 x 6.5	6323	250 x 250 x 6.3*	90	237.0	0	680	HF	-
Platt/82	Nottingham	X-RR-60-C	250.4 x 250.7 x 6.5	6323	250 x 250 x 6.3*	60	237.0	0	672	HF	-
Platt/82	Nottingham	X-RR-45-C	251.2 x 250.4 x 6.7	6518	250 x 250 x 6.3*	45	228.0	0	846	HF	-
Peksa/82	Nottingham	10P	99.2 x 99.2 x 4	1517	99.2 x 99.2 x 4	90	304.0	0	276	HF	-
Peksa/82	Nottingham	11P	99.3 x 99.3 x 4	1519	99.3 x 99.3 x 4	90	304.0	131.7	271	HF	-

Table 8. 77 Tests on Full-Width, Compression-Loaded, RHS X-connections, with Welded Branches

Researcher / year	Location	Specimen no.	b_0 x h_0 x t_0 [mm]	A_0 [mm^2]	b_1 x h_1 x t_1 [mm][1,2]	θ_1 [°][2]	f_{y0} [MPa][3]	f_0 [MPa][4]	N_{1u} [kN]	Forming process[5]	Failure mode
Peksa/82	Nottingham	12P	99.3 x 99.3 x 4	1519	99.3 x 99.3 x 4	90	304.0	263.3	275	HF	-
Peksa/82	Nottingham	13P	99.3 x 99.3 x 4	1519	99.3 x 99.3 x 4	90	304.0	263.3	280	HF	-
Peksa/82	Nottingham	14P	99.2 x 99.2 x 4	1517	99.2 x 99.2 x 4	90	304.0	197.8	271	HF	-
Peksa/82	Nottingham	15P	99.2 x 99.2 x 4	1517	99.2 x 99.2 x 4	90	304.0	65.9	263	HF	-
Bettison/82	Nottingham	5B	99.6 x 99.6 x 4.2	1596	99.6 x 99.6 x 4.2	90	336.0	237.5	313	HF	-
Bettison/82	Nottingham	6B	99.8 x 99.8 x 4.1	1563	99.8 x 99.8 x 4.1	90	336.0	255.3	284	HF	-
Poloni/85	Toronto	PWL 2	102.4 x 252.7 x 4.44	2886	100 x 50	90	388.0	0	242	CFSR	Bearing
Poloni/85	Toronto	PWL 4	102.4 x 252.7 x 4.44	2886	101 x 101	90	388.0	0	327	CFSR	Buckling
Poloni/85	Toronto	PWL 7	102.4 x 252.7 x 4.44	2886	101 x 177	90	388.0	0	390	CFSR	Buckling
Poloni/85	Toronto	PWL 10	102.4 x 252.7 x 4.44	2886	101 x 254	90	388.0	0	500	CFSR	Buckling
Poloni/85	Toronto	PWL 15	102.4 x 252.7 x 4.44	2886	101 x 381	90	388.0	0	674	CFSR	Buckling
Poloni/85	Toronto	PWS 2	252.7 x 102.4 x 4.44	2886	252 x 51	90	388.0	0	267	CFSR	Bearing
Poloni/85	Toronto	PWS 4	252.7 x 102.4 x 4.44	2886	253 x 102	90	388.0	0	407	CFSR	Buckling
Poloni/85	Toronto	PWS 7	252.7 x 102.4 x 4.44	2886	253 x 177	90	388.0	0	561	CFSR	Buckling
Poloni/85	Toronto	PWS 10	252.7 x 102.4 x 4.44	2886	254 x 254	90	388.0	0	822	CFSR	Buckling
Poloni/85	Toronto	PWS 15	252.7 x 102.4 x 4.44	2886	255 x 381	90	388.0	0	1149	CFSR	Buckling
Poloni/85	Toronto	PWLR	102.4 x 252.7 x 4.44	2886	102.4 x 252.7 x 4.44	90	388.0	0	438	CFSR	Buckling
Cheng/16	Sheffield	X1	100.5 x 100.3 x 2.92	1044	100.2 x 100.3 x 2.73	90	330.0	0	176	CF	Buckling
Cheng/16	Sheffield	X2	100.4 x 100.1 x 3.84	1317	100.4 x 100.2 x 3.69	90	330.0	0	302	CF	Buckling
Cheng/16	Sheffield	X3	100.3 x 99.8 x 4.89	1598	100.1 x 99.9 x 4.7	90	400.0	0	373	CF	Buckling
Cheng/16	Sheffield	X4	99.6 x 99.6 x 5.8	1802	99.8 x 99.7 x 5.46	90	370.0	0	560	CF	Buckling
Cheng/16	Sheffield	X5	99.9 x 99.7 x 7.92	2213	100.1 x 99.6 x 7.68	90	345.0	0	783	CF	Buckling
Cheng/16	Sheffield	X6	149.8 x 250 x 5	3620	150.1 x 150.1 x 4.76	90	463.0	0	409	CF	Buckling

Table 8. 77 Tests on Full-Width, Compression-Loaded, RHS X-connections, with Welded Branches

Researcher / year	Location	Specimen no.	b_0 x h_0 x t_0 [mm]	A_0 [mm^2]	b_1 x h_1 x t_1 [mm][1,2]	θ_1 [^{0}][2]	f_{y0} [MPa][3]	f_0 [MPa][4]	N_{1u} [kN]	Forming process[5]	Failure mode
Cheng/16	Sheffield	X7	150.2 x 150.2 x 5.86	3001	150.5 x 150.4 x 5.86	90	451.0	0	828	CF	Buckling
Cheng/16	Sheffield	X8	250.7 x 350.4 x 9.94	10456	248.5 x 249 x 9.94	90	468.0	0	-	CF	Buckling
Cheng/16	Sheffield	X9	300 x 400 x 7.92	10139	300.3 x 300.3 x 7.97	90	481.0	0	1289	CF	Buckling
Serrano/17	Oviedo	100x100x6-C100/8-S1	100.2 x 100.5 x 6.12	1890	99.8 x 8.1 x 8.1	90	500.0	0	219	CF	Bearing
Serrano/17	Oviedo	150x100x6-C100/8-S1	100.1 x 150 x 5.73	2371	9.1 x 8.01 x 8.01	90	454.0	0	242	CF	Bearing
Serrano/17	Oviedo	150x100x4-C100/8-S2	99.7 x 150.1 x 3.75	1663	99.5 x 8.07 x 8.07	90	369.0	0	143	CF	Bearing
Serrano/17	Oviedo	200x100x4-C100/8-S2	100.1 x 200 x 3.75	2038	99.8 x 7.99 x 7.99	90	447.0	0	154	CF	Bearing
Serrano/17	Oviedo	150x100x4-C100/8-S3	99.9 x 150 x 3.78	1673	99.7 x 7.96 x 7.96	90	369.0	0	151	CF	Bearing

Table 9. 28 Tests on Full-Width, Compression-Loaded, RHS X-connections, with Branches Welded on One Side

Researcher / year	Location	Specimen no.	b_0 x h_0 x t_0 [mm]	A_0 [mm^2]	b_1 x h_1 x t_1 [mm][1,2]	θ_1 [°][2]	f_{y0} [MPa][3]	f_0 [MPa][4]	N_{1u} [kN]	Forming process[5]	Failure mode
Barentse/77	Delft	T-RR-A-A-1	101.4 x 101.4 x 6.23	2343	101.4 x 101.4 x 6.23	90	299.0	0	417	HF	Buckling
Barentse/77	Delft	T-RR-A-A-7	101.3 x 101.3 x 4.03	1431	100.2 x 100.2 x 3.77	90	326.3	0	210	HF	Buckling
Barentse/77	Delft	T-RR-A-A-10	100.4 x 100.4 x 2.88	1063	100.4 x 100.4 x 2.88	90	299.3	0	112	HF	Buckling
Barentse/77	Delft	T-RR-E-A-94	101.8 x 50.9 x 4.73	1332	101.8 x 50.9 x 4.73	90	337.7	0	298	HF	Buckling
Barentse/77	Delft	T-RR-E-A-97	101.3 x 51 x 3.35	959	101.3 x 51 x 3.35	90	293.0	0	150	HF	Buckling
Barentse/77	Delft	T-RR-E-A-112	102.1 x 151.3 x 6.23	2946	101.4 x 101.4 x 6.18	90	288.5	0	394	HF	Buckling
Barentse/77	Delft	T-RR-E-A-119	101.2 x 151.4 x 4.82	2320	101.4 x 101.4 x 6.23	90	293.0	0	256	HF	Buckling
Barentse/77	Delft	T-RR-E-A-126	80.6 x 119.7 x 3.05	1145	80.2 x 80.2 x 3	90	397.5	0	142	CF	Buckling
Barentse/77	Delft	T-RR-C-A-46	100.2 x 100.2 x 3.77	1435	100 x 40.3 x 3.08	90	349.0	0	180	HF	Buckling
Barentse/77	Delft	T-RR-C-A-50	100.8 x 100.8 x 3.36	1271	100 x 40.3 x 3.02	90	289.6	0	152	HF	Buckling
Barentse/77	Delft	T-RR-C-A-45	101 x 101 x 4	1422	100.9 x 75.4 x 3.92	90	343.2	0	248	HF	Buckling
Barentse/77	Delft	T-RR-C-A-49	100.8 x 100.8 x 3.36	1271	99.8 x 80.5 x 4	90	289.6	0	162.5	HF	Buckling
Barentse/77	Delft	T-RR-G-A-211	101.4 x 101.4 x 6.23	2343	101.4 x 101.4 x 6.23	90	299.0	120	419	HF	Buckling
Barentse/77	Delft	T-RR-G-A-214	101.3 x 101.3 x 4.03	1431	100.2 x 100.2 x 3.77	90	326.3	131	209	HF	Buckling
Barentse/77	Delft	T-RR-G-A-217	100.4 x 100.4 x 2.88	1063	100.4 x 100.4 x 2.88	90	299.0	119	107	HF	Buckling
Barentse/77	Delft	T-RR-G-A-201	101.4 x 101.4 x 6.23	2340	101.4 x 101.4 x 6.23	90	299.0	209.4	360	HF	Buckling
Barentse/77	Delft	T-RR-G-A-204	101 x 101 x 4	1420	101 x 101 x 4	90	343.2	274.6	199	HF	Buckling
Barentse/77	Delft	T-RR-G-A-207	100.4 x 100.4 x 2.88	1063	100.4 x 100.4 x 2.88	90	299.0	238.9	110	HF	Buckling
Zhao/91	Sydney	S1B1C11	51 x 102 x 4.9*	1342	51 x 51 x 4.9*	90	409.2	0	316	CF	Buckling
Zhao/91	Sydney	S1B1C12	51 x 102 x 3.2*	912	51 x 51 x 4.9*	90	344.6	0	163	CF	Buckling
Zhao/91	Sydney	S1B2C21	102 x 102 x 9.5*	3283	102 x 102 x 8*	90	444.8	0	1207	CF	Buckling
Zhao/91	Sydney	S1B2C22	102 x 102 x 6.3*	2309	102 x 102 x 8*	90	432.6	0	652	CF	Buckling
Zhao/91	Sydney	S3B1C11A1	51 x 102 x 4.9*	1342	51 x 51 x 4.9*	90	409.2	321.8	312	CF	Buckling

Table 9. 28 Tests on Full-Width, Compression-Loaded, RHS X-connections, with Branches Welded on One Side

Researcher / year	Location	Specimen no.	b_0 x h_0 x t_0 [mm]	A_0 [mm^2]	b_1 x h_1 x t_1 [mm][1,2]	θ_1 [^{0}][2]	f_{y0} [MPa][3]	f_0 [MPa][4]	N_{1u} [kN]	Forming process[5]	Failure mode
Zhao/91	Sydney	S3B1C11A0.5	51 x 102 x 4.9*	1342	51 x 51 x 4.9*	90	409.2	116.1	320	CF	Buckling
Zhao/91	Sydney	S3B1C12A1	51 x 102 x 3.2*	912	51 x 51 x 4.9*	90	344.6	304.9	156	CF	Buckling
Zhao/91	Sydney	S3B1C12A0.5	51 x 102 x 3.2*	912	51 x 51 x 4.9*	90	344.6	125	161	CF	Buckling
Fan/2017	Toronto	X-1.0-32-700O	203.6 x 203.6 x 5.96	4492	204 x 204 x 11.67	90	403.9	0	653	CF	Buckling
Fan/2017	Toronto	X-1.0-21-550O	203.1 x 203.1 x 8.85	6495	204 x 204 x 11.67	90	417.5	0	1264	CF	Buckling

Table 10. 20 Tests on Full-Width, Compression-Loaded, RHS X-connections, with Unwelded Branches

Researcher / year	Location	Specimen no.	b_0 x h_0 x t_0 [mm]	A_0 [mm^2]	b_1 x h_1 x t_1 [mm][1,2]	θ_1 [^{0}][2]	f_{y0} [MPa][3]	f_0 [MPa][4]	N_{1u} kN]	Forming process[5]	Failure mode
Poloni/85	Toronto	PUL 4	102.4 x 252.7 x 4.44	2886	101 x 101	90	388.0	0	165	CFSR	Buckling
Poloni/85	Toronto	PUL 7	102.4 x 252.7 x 4.44	2886	102 x 178	90	388.0	0	193	CFSR	Buckling
Poloni/85	Toronto	PUS 4	252.7 x 102.4 x 4.44	2886	255 x 103	90	388.0	0	161	CFSR	Buckling
Poloni/85	Toronto	PUS 7	252.7 x 102.4 x 4.44	2886	255 x 177	90	388.0	0	192	CFSR	Buckling
Zhao/91	Sydney	S1P1C11	51.6 x 103 x 4.73	1315	51 x 51	90	446.8	0	203	CF	Buckling
Zhao/91	Sydney	S1P1C12	51.1 x 102.5 x 3.15	903	51 x 51	90	436.4	0	102	CF	Buckling
Zhao/91	Sydney	S1P2C11	51.3 x 102.9 x 4.72	1308	51 x 25.5	90	446.8	0	186	CF	Buckling
Zhao/91	Sydney	S1P2C12	51 x 102.6 x 3.16	905	51 x 25.5	90	436.4	0	91.4	CF	Buckling
Zhao/91	Sydney	S1P3C21	102.5 x 102.4 x 9.63	3338	102 x 102	90	496.1	0	946	CF	Buckling
Zhao/91	Sydney	S1P3C22	101.8 x 101.8 x 6.1	2240	102 x 102	90	445.2	0	475	CF	Buckling
Zhao/91	Sydney	S1P4C21	102.5 x 102.4 x 9.65	3342	102 x 51	90	496.2	0	818	CF	Buckling
Zhao/91	Sydney	S1P4C22	101.9 x 101.9 x 6.09	2238	102 x 51	90	445.2	0	384	CF	Buckling
Zhao/91	Sydney	S3P1C11A1	51.4 x 102.3 x 4.72	1304	51 x 51	90	446.8	345.3	148	CF	Buckling
Zhao/91	Sydney	S3P1C11A0.5	51.4 x 102.7 x 4.74	1313	51 x 51	90	446.8	189.3	189	CF	Buckling
Zhao/91	Sydney	S3P1C12A1	50.7 x 102.5 x 3.17	905	51 x 51	90	436.5	334.7	73.9	CF	Buckling
Zhao/91	Sydney	S3P1C12A0.5	50.9 x 102.2 x 3.15	900	51 x 51	90	436.4	190.9	93	CF	Buckling
Zhao/91	Sydney	S3P2C11A1	51.5 x 102.5 x 4.73	1309	51 x 25.5	90	446.8	332.8	122	CF	Buckling
Zhao/91	Sydney	S3P2C11A0.5	51.2 x 102.3 x 4.73	1305	51 x 25.5	90	446.9	215.8	168	CF	Buckling
Zhao/91	Sydney	S3P2C12A1	50.8 x 102.3 x 3.17	905	51 x 25.5	90	436.5	322.5	60.6	CF	Buckling
Zhao/91	Sydney	S3P2C12A0.5	50.8 x 102.3 x 3.17	904	51 x 25.5	90	436.5	204.0	80	CF	Buckling

[1] b_1 x h_1 x t_1 for RHS branch, where $h_1 = t_1$ for plate branch; b_1 x h_1 for branch using steel block or bearing plate

[2] Based on upper branch dimensions (which are equal or almost equal to the bottom branch dimensions, except when only an upper branch is used)

[3] For further clarification of mechanical properties see Fan (2017)

[4] Compressive stress in chord connecting face due to both chord axial force and/or moment

[5] HF: hot-formed; CF: cold-formed; CFSR: cold-formed stress-relieved

Notes: All values are measured properties unless specified with *; "-" indicates data that is not available

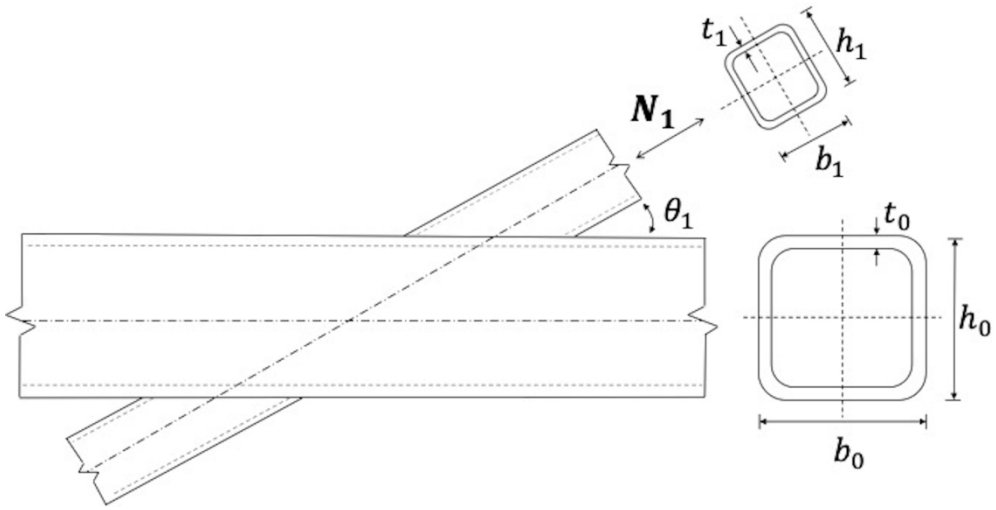

Figure 1.

239x120mm (300 x 300 DPI)

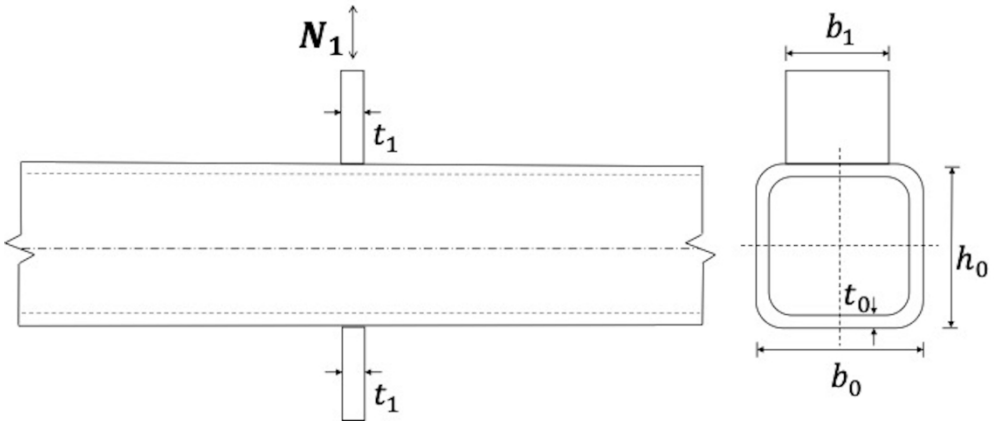

Figure 2.

239x101mm (300 x 300 DPI)

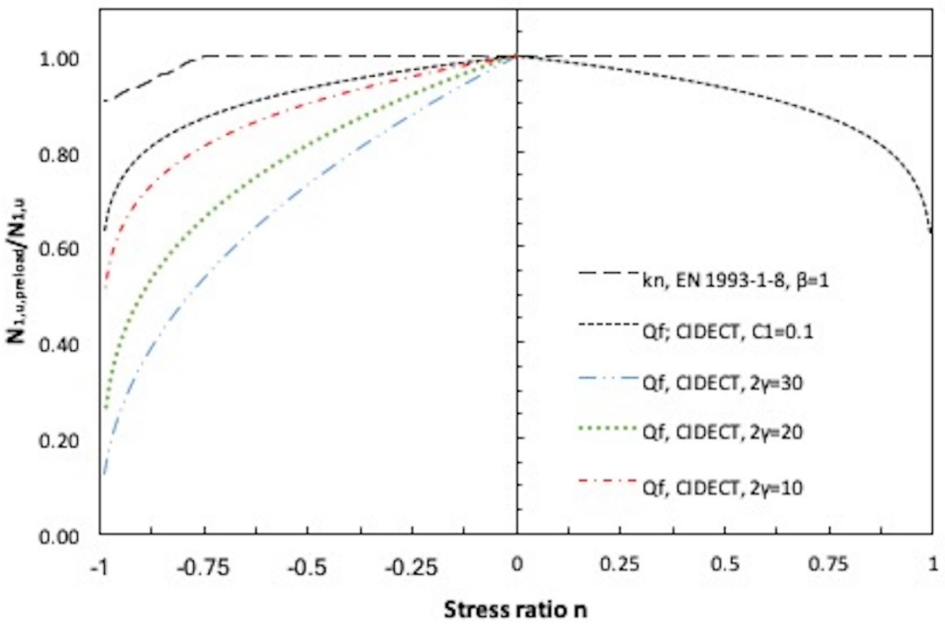

Figure 3.

158x107mm (300 x 300 DPI)

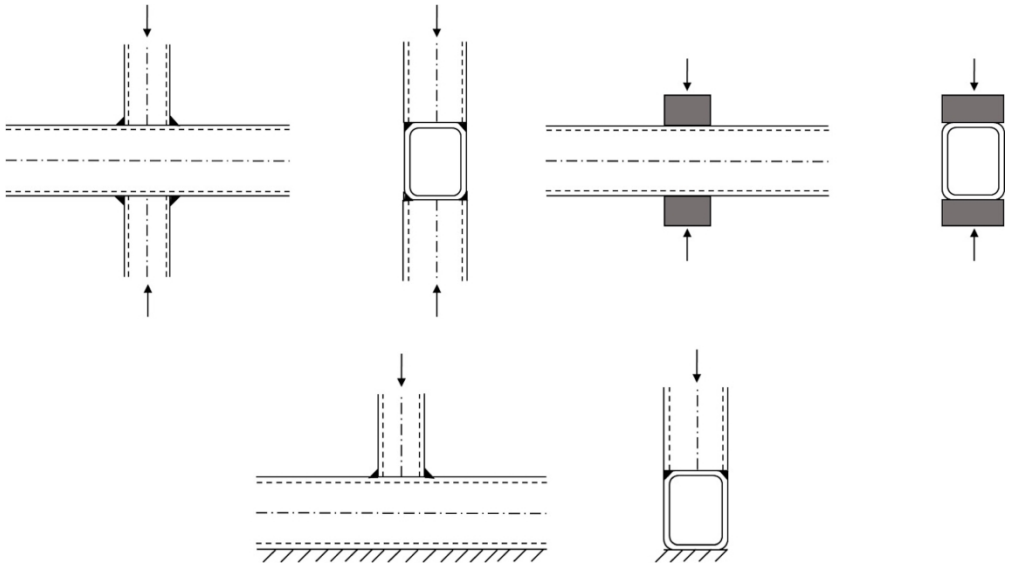

Figure 4.

511x286mm (300 x 300 DPI)

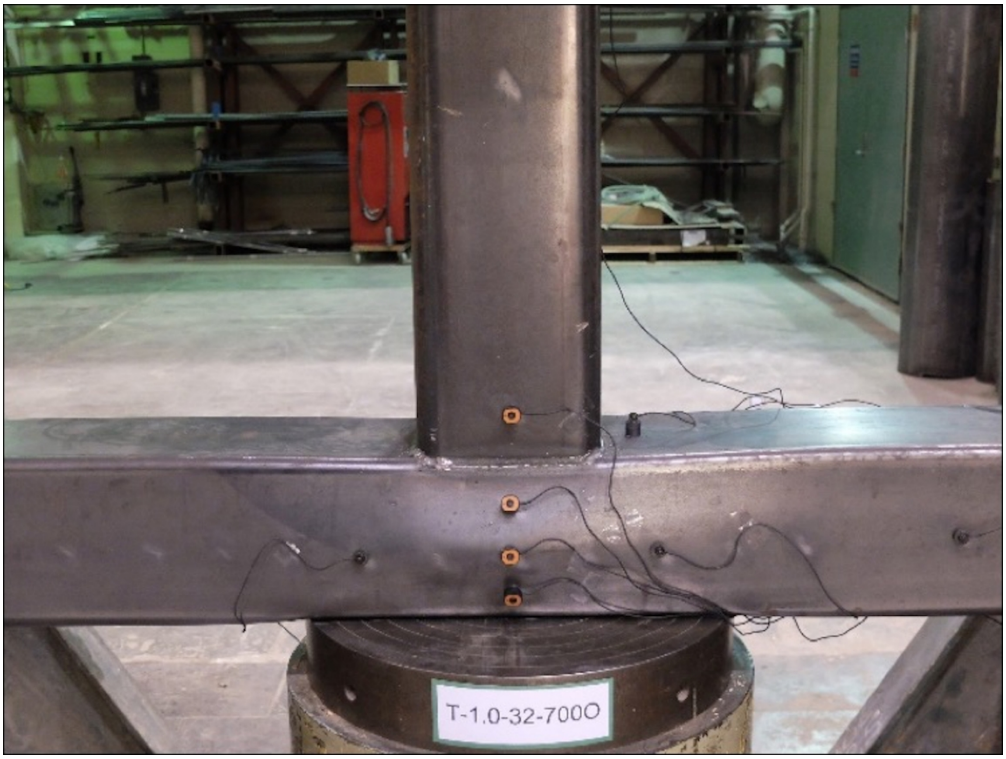

Figure 5.

262x197mm (300 x 300 DPI)

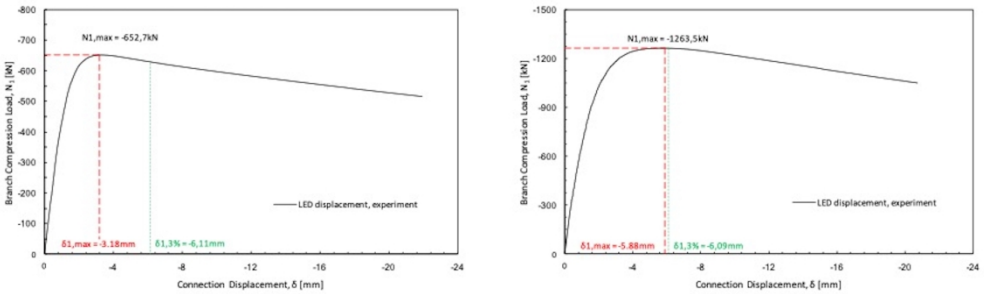

Figure 6.

302x92mm (300 x 300 DPI)

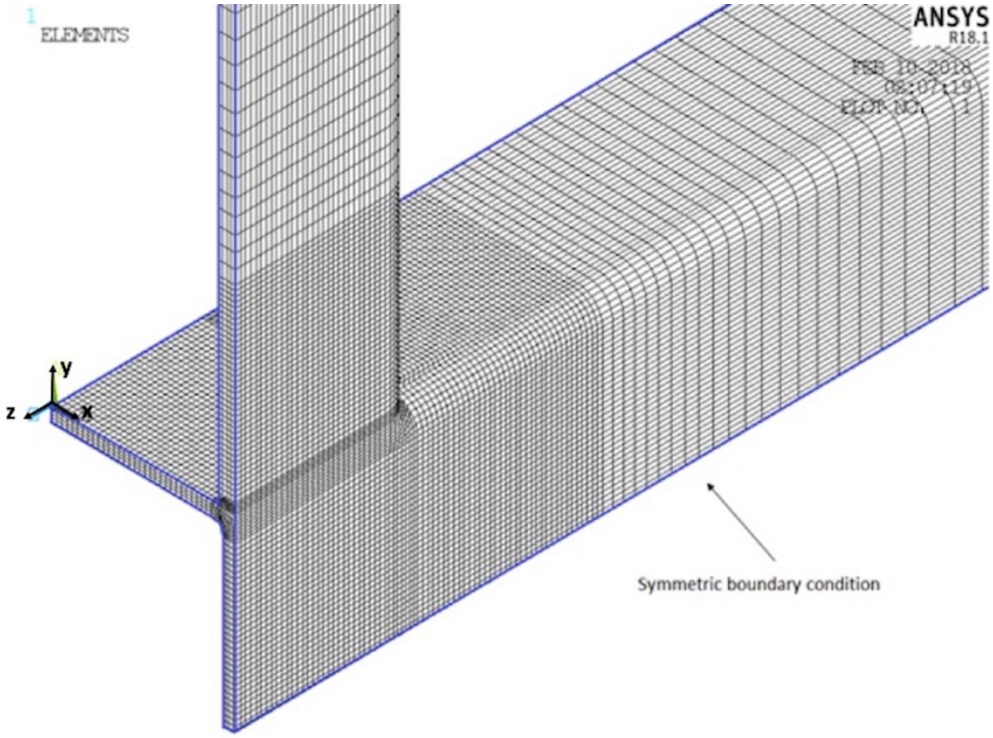

Figure 7.

255x190mm (300 x 300 DPI)

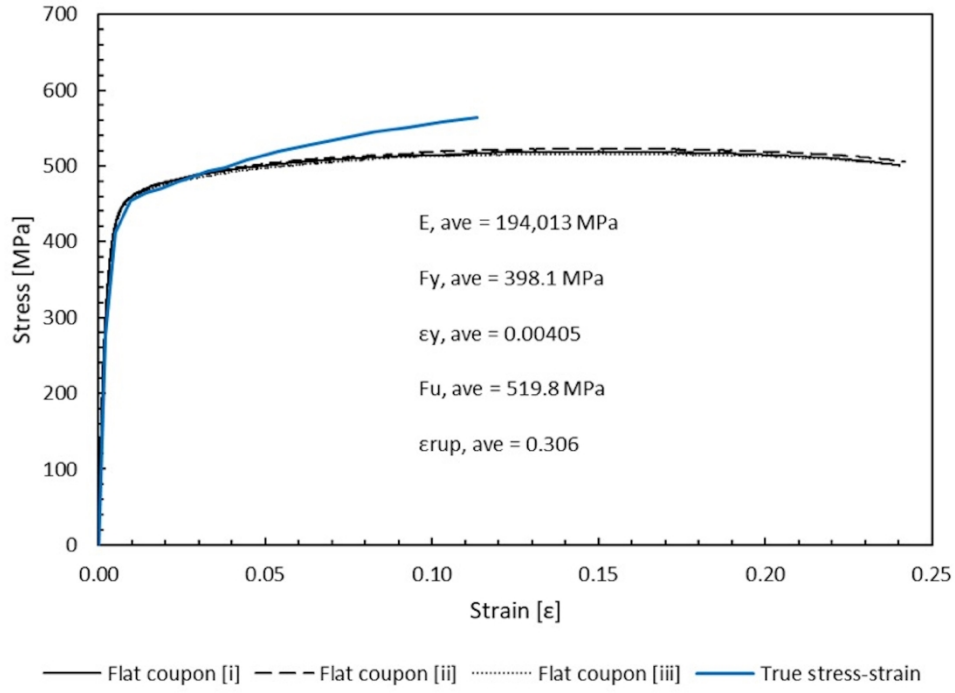

Figure 8.

309x222mm (300 x 300 DPI)

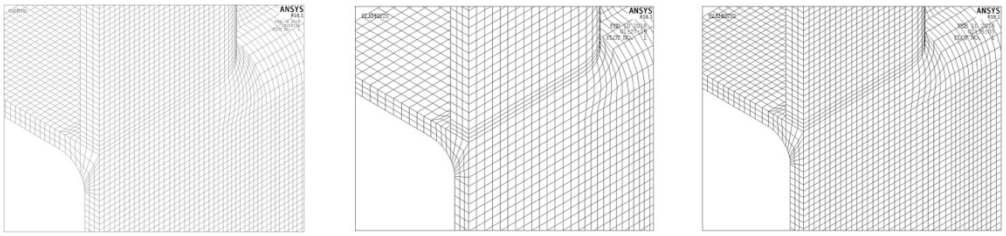

Figure 9.

495x113mm (300 x 300 DPI)

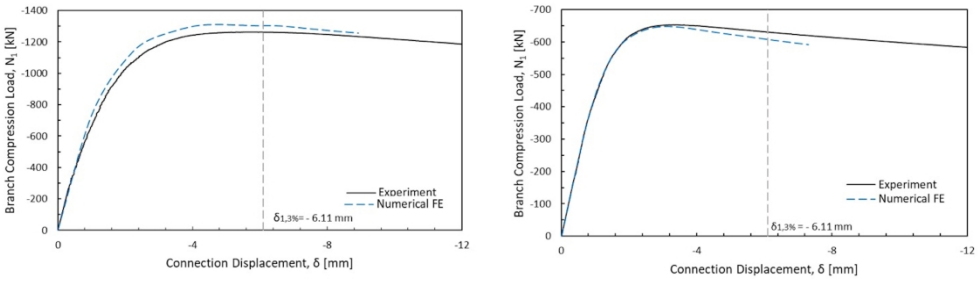

Figure 10.

521x149mm (300 x 300 DPI)

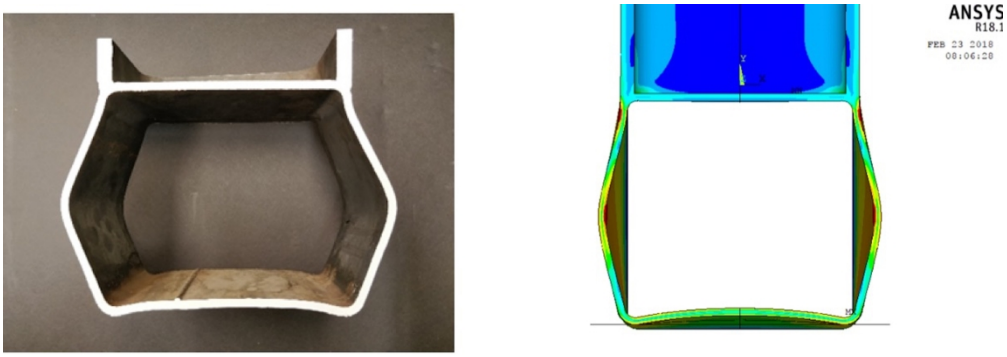

Figure 11.

428x149mm (300 x 300 DPI)

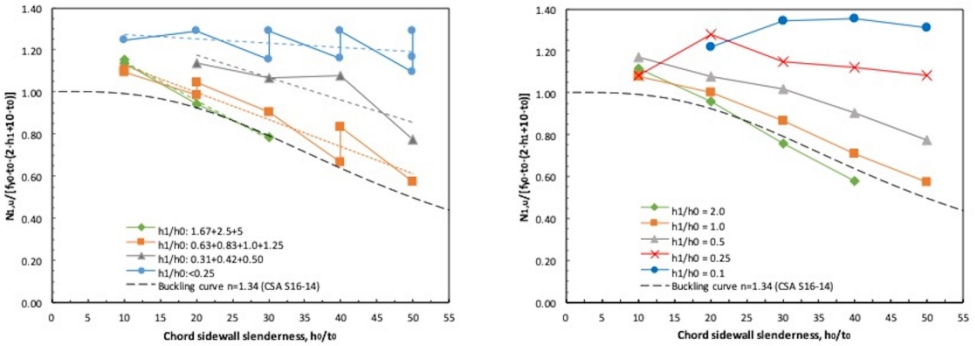

Figure 12.

302x110mm (300 x 300 DPI)

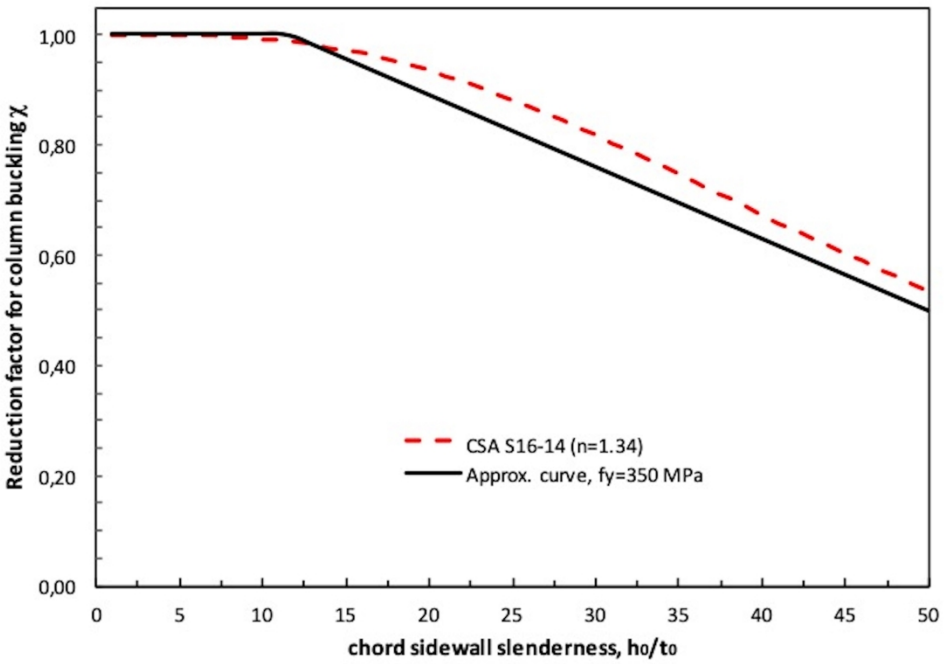

Figure 13.

254x182mm (300 x 300 DPI)

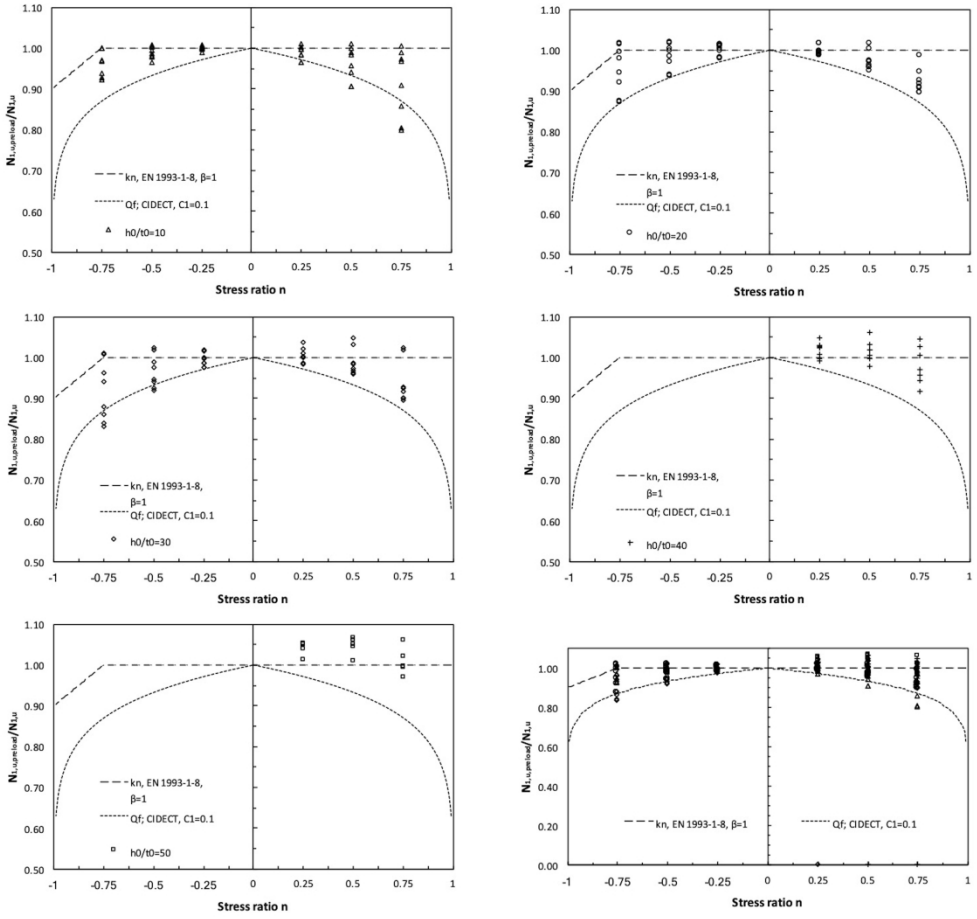

Figure 14.

529x494mm (300 x 300 DPI)

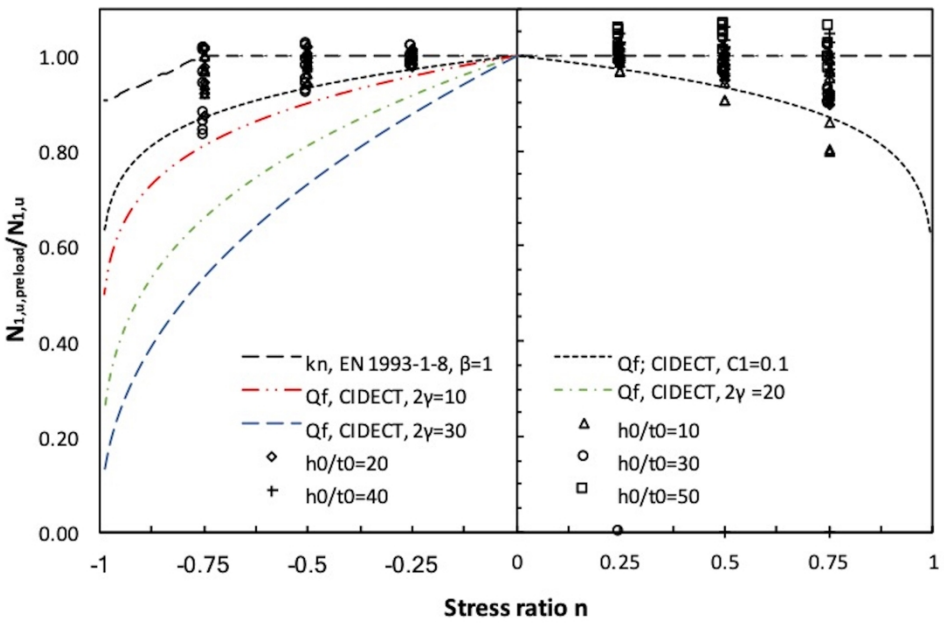

Figure 15.

300x203mm (300 x 300 DPI)

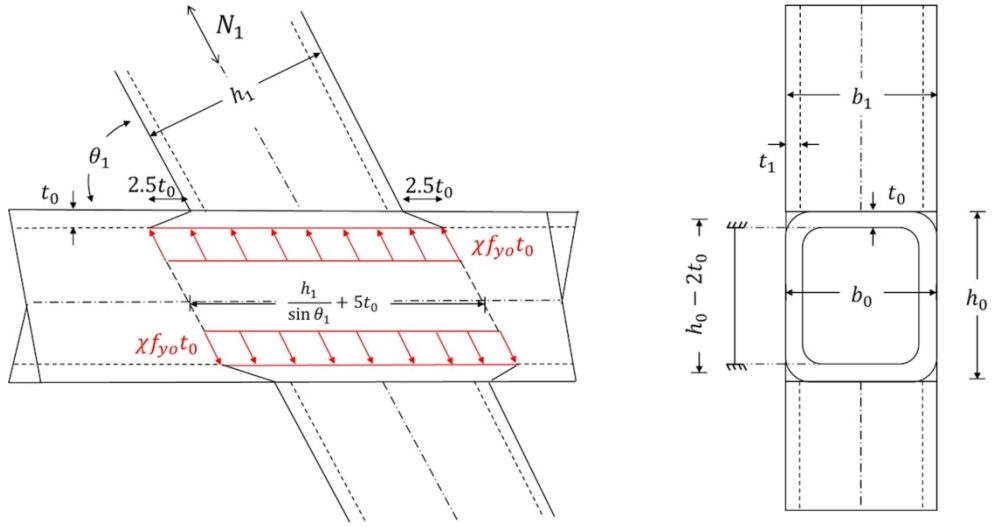

Figure 16.

436x228mm (300 x 300 DPI)

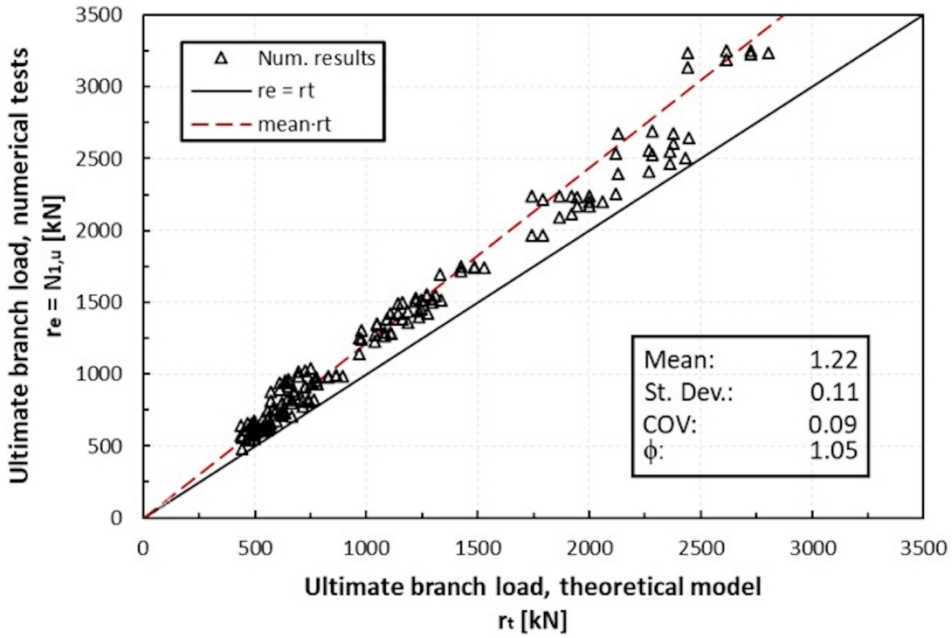

Figure 17.

245x165mm (300 x 300 DPI)

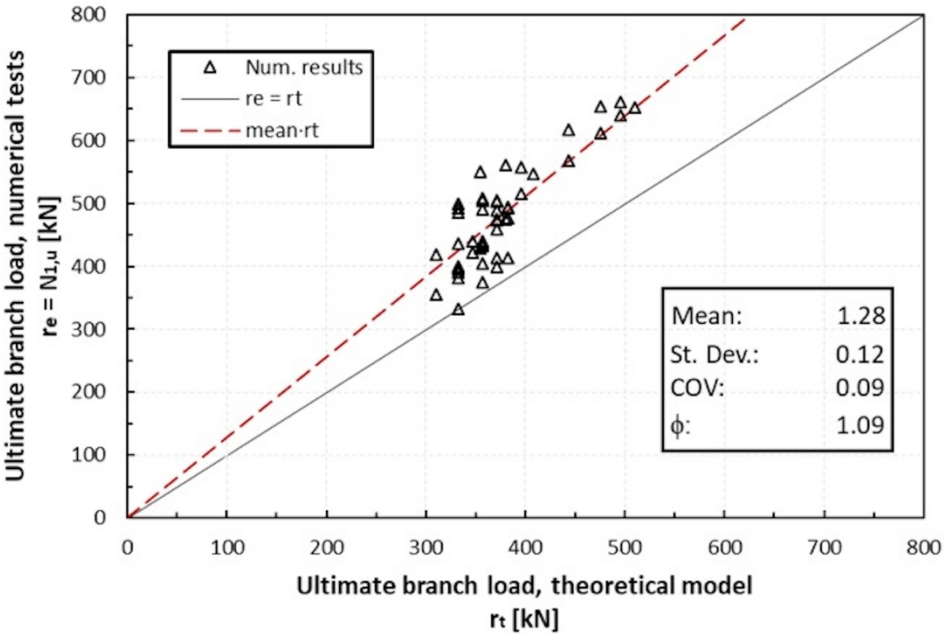

Figure 18.

245x165mm (300 x 300 DPI)

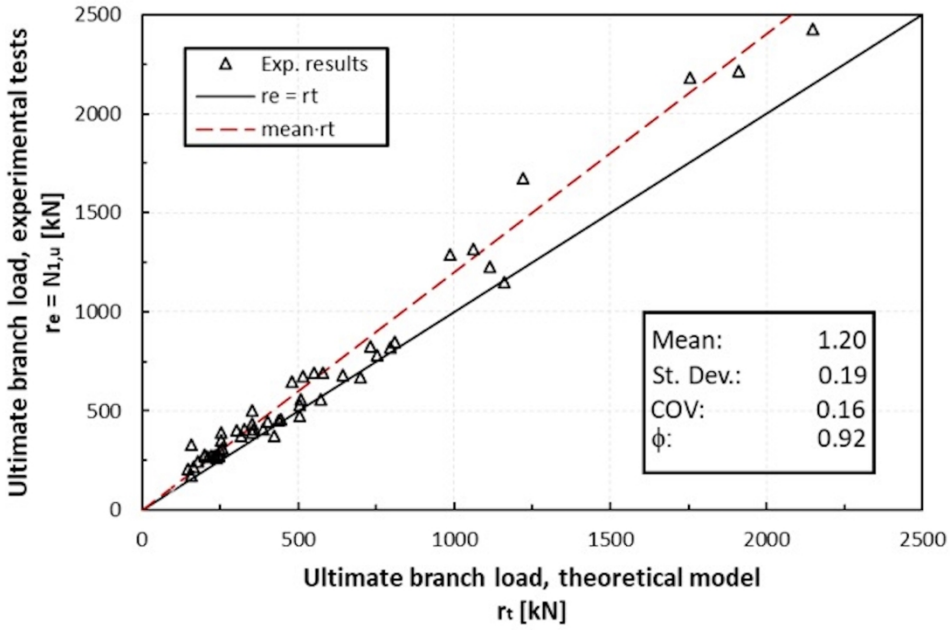

Figure 19.

245x163mm (300 x 300 DPI)

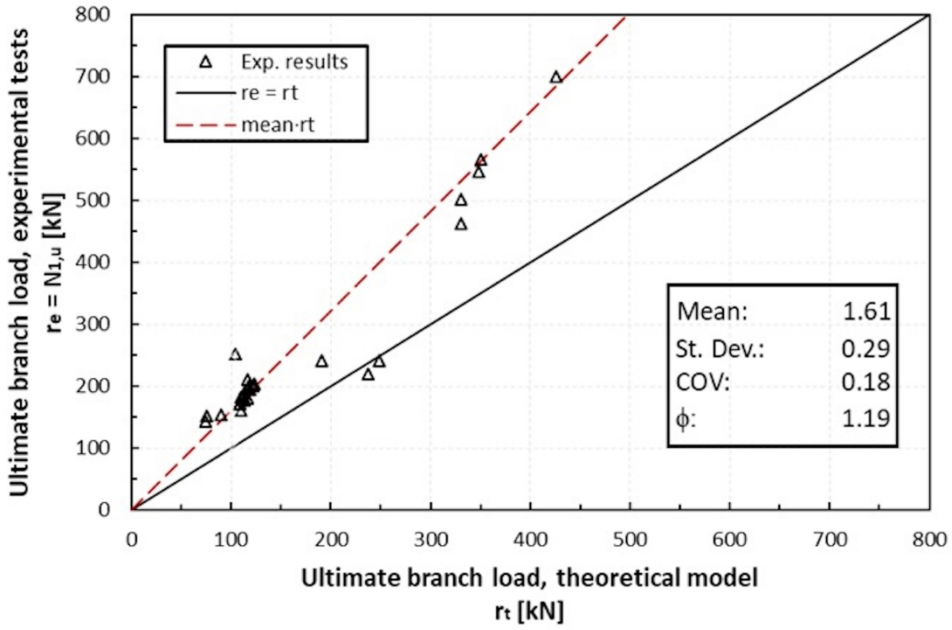

Figure 20.

245x163mm (300 x 300 DPI)

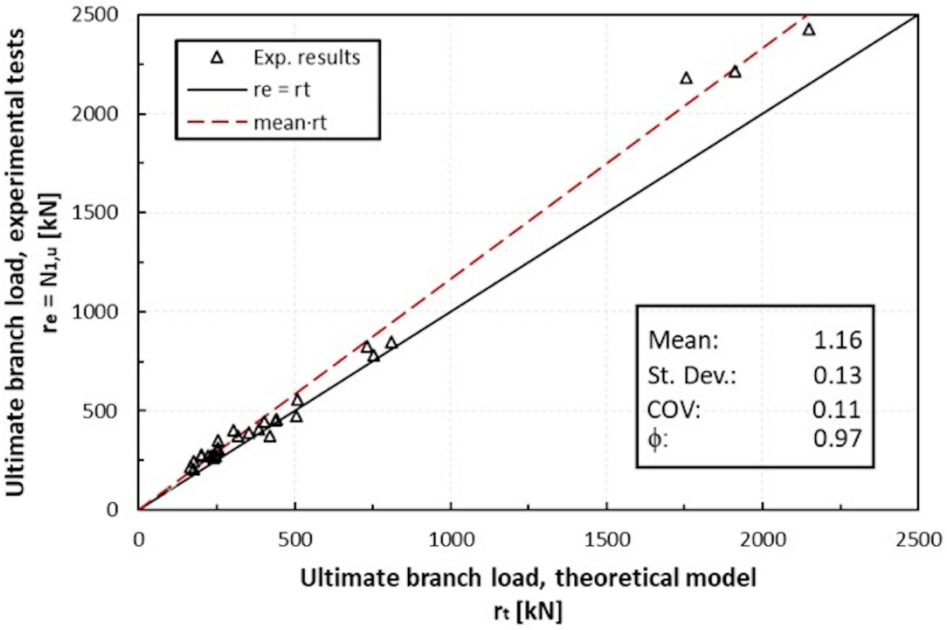

Figure 21.

245x163mm (300 x 300 DPI)

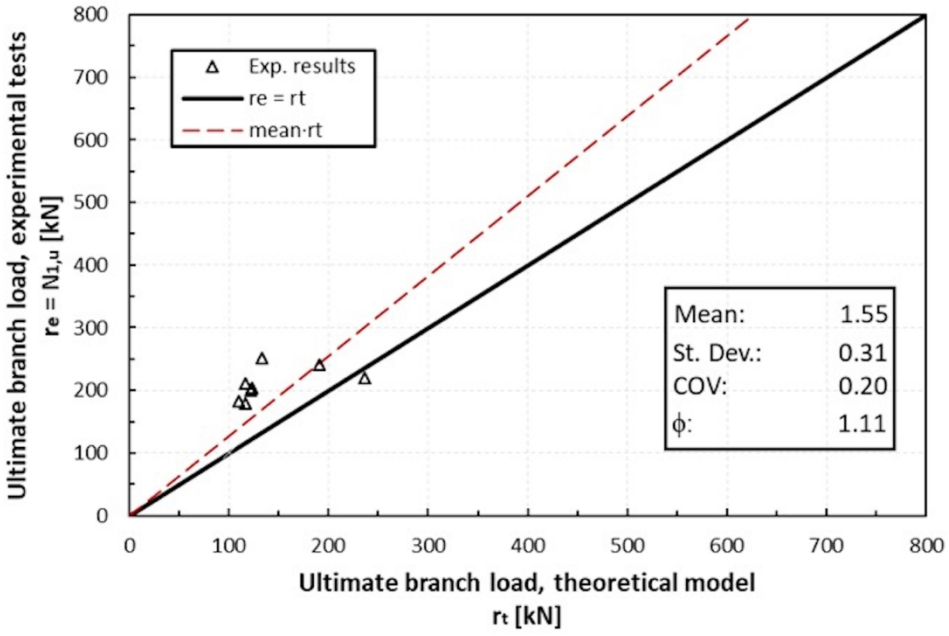

Figure 22.

245x165mm (300 x 300 DPI)